

POLITECNICO DI TORINO

Master Degree in Mechanical Engineering



Green Engine for Air Transport



Study of new simulation method for a LP turbine row, trade-off study and assessment

Academic supervisor:
Prof. Paolo Maggiore

Internal supervisor:
Eng. Paride Mesaglio Chittaro
Eng. Witold Szwed

Candidate:
Luca Cipressa

Abstract

The aim of this work is to develop a multidisciplinary tool able to give fast aeromechanic feedback in preliminary design of LPT stages of aeronautical engines. What represents a high performance system from the aerodynamic point of view might be not feasible from aeromechanic side: this leads to iterations which slow down the workflow and drive to misunderstandings and errors.

The tool workflow starts from the airfoil geometry, defined during the aerodynamic optimization. In the first place, a representative CAD model of the stage is created. It is used to generate a FE model with realistic boundary conditions. Finally a modal analysis is run to assess the vibratory behavior of the stage on a Campbell diagram.

To speed up and strengthen the process, a wizard in *ANSYS Workbench* environment has been developed in order to automatically perform the modal analysis for a vane stage, from the mesh generation up to modeshapes classification, passing through BCs setup. Many possible approaches have been studied from qualitative and quantitative point of view, in order to define the best setup and get consistent results. Where necessary, useful *macros* have been developed for ANSYS Mechanical to refine the procedure.

The tool handles the geometry in *Unigraphics NX* workspace, where the profile is *easily* created thanks to a parametric approach. The CAD setup is managed by recalling another GUI internally developed in Avio Aero, *DynBooster*. The boundaries of the airfoil have been treated by means of parametric templates, optimized in order to always supply realistic geometries.

This way, many aerodynamic profiles can be quickly and easily assessed from dynamic standpoint to fast figure out the result robustness from mechanical point of

view too.

The procedure has been refined first for the nozzle, since it represents the simplest model to analyze, and it demonstrated a deep reduction of the processing time - up to 90% - figuring out consistent advantages. This suggested the possibility of implementing more complex models such as the *bladed disc* and, thus, apply the tool not only in a preliminary design phase, but also for a detailed aeromechanics assessment. To pave the way to the automatic analysis of the realistic rotor stage, a study on a simplified blade model has been conducted and tested with the tool.

Acknowledgments

I want to thank first the ATO team of Avio Aero leded by eng. Paolo Calza who trusted my skills letting me to face my first job experience. More in detail, my deepest gratitude is towards eng. Marco Moletta, eng. Paride Mesaglio Chittaro and eng. Witold Szwed who supervised me overall the entire workflow, teaching me *how things are done* in contrast to pure theory says. They gave me a way of thinking inside the job environment which surely will help me in my future career.

On the academic side, my most sincere gratitude goes to prof. Paolo Maggiore who followed me with critical point of view during the work, giving me all the theoretical background for the understanding of the outcoming results of the thesis.

Contents

Abstract	i
Acknowledgments	iii
List of Figures	viii
List of Tables	ix
Nomenclature	x
1 Introduction	1
1.1 Project <i>GREAT 2020</i>	1
1.1.1 The actors of the project	2
1.2 Thesis overview	4
2 The aeronautical engine	7
2.1 Main architectures in service	7
2.1.1 Turbofan	8
2.1.2 Turboprop	9
2.1.3 Turboshaft	10
2.2 Low Pressure Turbine	10
2.2.1 LPT row	11
3 Dynamics and aeromechanics concepts for LPT	14
3.1 Excitation on the bladed disc	16
3.1.1 The forced response	17
3.1.2 Flutter	18

3.2	Modal analysis	19
3.2.1	Modeshapes of a bladed disc	21
3.2.2	Different modal shape families	23
3.2.3	Campbell diagram	26
3.2.4	Modal Assurance Criterion	28
4	Rotors in cyclic symmetry	30
5	The design of LPT stage	35
5.1	The aerodynamic design	37
5.2	The preliminary mechanical design	39
5.3	The Aero-Mech design concept	41
5.3.1	<i>PRIME</i> overview	42
6	Validation of <i>Workbench</i> procedure	45
6.1	Vane	46
6.2	Simplified Blade	50
6.3	Bladed disc	53
6.3.1	Tight Interlocking	58
6.3.2	Radial Free	60
6.3.3	Single Point	61
6.3.4	Tip Free	62
7	The tool <i>PRIME</i>	65
7.1	The parametric templates for Vane model	65
7.1.1	How to generate a template	66
7.1.2	The tool <i>DynBooster</i>	67
7.2	The WB wizard for <i>FEM</i>	72
7.3	Vane in <i>PRIME</i>	76
7.4	Blade Only in <i>PRIME</i>	78
	Conclusions	81
	References	83

List of Figures

1.1.1 <i>ACARE</i> goals for MY 2020	1
1.2.1 Design workflow of a blade profile	5
2.1.1 Turbojet architecture	8
2.1.2 Turbofan architecture	8
2.1.3 Turboprop architecture	9
2.1.4 Turboshaft architecture	10
2.2.1 GE90 architecture, double shaft turbofan engine	11
2.2.2 Vane segment	12
2.2.3 Rotor blade on the left, tip shroud enlargement on the right	13
3.0.1 Failure of Tacoma bridge	15
3.0.2 Example of bladed disc mounted on the shaft	15
3.1.1 Triangle of the aeroelasticity	16
3.1.2 Interaction of the stator and rotor stage	17
3.1.3 Example of Campbell diagram	18
3.1.4 Example of aeroplots, below the 0 damping is negative, thus, the system is unstable	19
3.2.1 Example of multi degrees of freedom system	20
3.2.2 Example of a 12 blades rotor modeshapes	21
3.2.3 Bladed disc, Nodal Diameter 1, forward wave	22
3.2.4 Bladed disc, Nodal Diameter 1, backward wave	23
3.2.5 Example of FreND diagram	24
3.2.6 Edgewise	25
3.2.7 Flapwise	25

3.2.8 Bending	26
3.2.9 Torsion	26
3.2.10 Example of Campbell diagram: crossings EO/modeshapes are potentially resonance conditions	27
4.0.1 Bladed disc row and single sector	31
4.0.2 Cyclic interfaces of the bladed disc	31
5.0.1 LPT cross section	36
5.1.1 Velocity triangles for a turbine stage	37
5.1.2 Airfoil nomenclature	38
5.2.1 Boundaries of the airfoil	39
5.2.2 Design workflow of a blade profile	40
5.3.1 Aero-Mech optimization	41
5.3.2 Design process improvement with the tool PRIME	42
6.0.1 Finite Element Model example	45
6.1.1 Vane profile of LPT	47
6.1.2 Boundaries and thermal load on Vane stage	48
6.1.3 1F	49
6.1.4 1T	49
6.1.5 2F	49
6.2.1 Blade profile of LPT	51
6.2.2 Cartesian, cylindrical and spherical frame in Ansys Workbench	52
6.3.1 Bladed disc profile of LPT with cyclic symmetry constraint	54
6.3.2 Extract solution log file, cyclic symmetry correctly set	56
6.3.3 Bladed disc under centrifugal load	57
6.3.4 Traveling wave on bladed disc row	58
7.1.1 Example of template	67
7.1.2 Airfoil generated through a set of 2D cross sections	68
7.1.3 Template centering	69
7.1.4 Template updating workflow	71

7.1.5 Parametric template for OBV	71
7.1.6 Parametric template for IBV	71
7.2.1 Model in WB through the Named Selection created in NX	73
7.2.2 Campbell diagram generated downstream the PRIME procedure	74
7.2.3 WB project automatically generated through the tool PRIME	75
7.2.4 PRIME workflow	76
7.4.1 Blade manually set with proper Named Selections	79

List of Tables

6.1	Relative error on frequency base between Nastran and WB model - vane	49
6.2	Relative error on frequency base between Nastran and WB model - blade only	52
6.3	Relative error on frequency base between Nastran and WB model - blisc - Tight Interlocking	59
6.4	Relative error on frequency base between Nastran and WB model - blisc - Radial Free	61
6.5	Relative error on frequency base between Nastran and WB model - blisc - Single Point	62
6.6	Relative error on frequency base between Nastran and WB model - blisc - Tip Free	63
7.1	Relative error on frequency base between Nastran and WB model - vane, manual grid	77
7.2	Relative error on frequency base between Nastran and PRIME model - vane, manual grid	77
7.3	Relative error on frequency base between Nastran and WB model - blade only, manual grid	79
7.4	Relative error on frequency base between Nastran and PRIME model - blade only, manual grid	80

Nomenclature

<i>1F</i>	<i>Bending mode</i>
<i>1T</i>	<i>Torsional mode</i>
<i>A/F</i>	<i>Air foil</i>
<i>BC</i>	<i>Boundary Condition</i>
<i>CAD</i>	<i>Computer Aided Design</i>
<i>CAE</i>	<i>Computer Aided Engineering</i>
<i>CFD</i>	<i>Computational Fluid Dynamics</i>
<i>CO₂</i>	<i>Carbon Anhydride</i>
<i>DB</i>	<i>DynBooster</i>
<i>dB</i>	<i>deciBell</i>
<i>dof</i>	<i>Degree Of Freedom</i>
<i>EW</i>	<i>Edgewise</i>
<i>FEA</i>	<i>Finite Elements Analysis</i>
<i>FEM</i>	<i>Finite Elements Model</i>
<i>FW</i>	<i>Flapwise</i>
<i>GUI</i>	<i>Graphical User Interface</i>
<i>HPC</i>	<i>High Pressure Compressor</i>
<i>HPT</i>	<i>High Pressure Turbine</i>
<i>IBPA</i>	<i>Interblade Phase Angle</i>
<i>IBV</i>	<i>Inner Band Vane</i>
<i>ISO</i>	<i>International Organization for Standardization</i>

<i>LPC</i>	<i>Low Pressure Compressor</i>
<i>LPT</i>	<i>Low Pressure Turbine</i>
<i>MPC</i>	<i>Multi Point Constraint</i>
<i>ND</i>	<i>Nodal Diameter</i>
<i>NO_x</i>	<i>Nitrogen Oxides</i>
<i>OBV</i>	<i>Outer Band Vane</i>
<i>R&D</i>	<i>Research and Development</i>
<i>SPC</i>	<i>Single Point Constraint</i>
<i>SW</i>	<i>Software</i>
<i>WB</i>	<i>Workbench</i>

Chapter 1

Introduction

1.1 Project *GREAT 2020*

In 2009 the research program *GREAT 2020* (**G**Reen **E**ngine for **A**ir **T**raffic) was born aiming to reach within the year 2020 the important goals proposed by the European Commission and *ACARE* (Advisory Council for Aviation Research and Innovation in Europe) such as the reduction of chemical and acoustic pollution of aircraft engines.

The major points are to halve the CO_2 emission, the decrease NO_x rate by 80% and lower the acoustic noise of 10 dB with respect to the legislation in act in 2000.

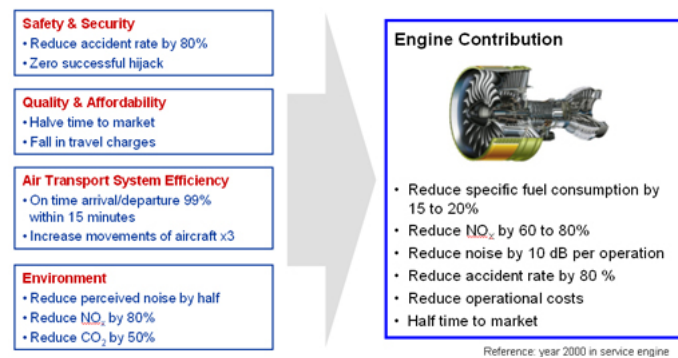


Figure 1.1.1: *ACARE* goals for MY 2020

The major constraint is not only to achieve the legislative limits, but to im-

prove the technology behind the design in order to go towards solutions that are respectful of environment and human health. As far as concerned the aeronautical engines, the main goal is the weight reduction and, so, get higher performance and pay load. It is, thus, necessary to push forward the technology limit by looking to more innovative design processes which allow to implement lighter and more resistant architectures.

This master thesis project is, so, thought with this idea to extend the limit of *low pressure turbine* stages design in order to build more efficient geometries; the most important goal is to merge the aerodynamic and aeromechanic process in one unique *AeroMech* concept.

1.1.1 The actors of the project

The city of Turin and the region Piedmont represent the main stages where the project *GREAT 2020* can be developed and get important results, thanks to the presence in the territory of many companies, small and large, in aeronautical field, excellence research centers and the high academic offer of the Politecnico di Torino.

These ingredients made possible the birth, in 2009, of the *Comitato Distretto Aerospaziale Piemonte* financially sustained by the region in order to answer to the technological requests and, furthermore, promote the creation of permanent R&D entities of aeronautical field.

The main actors of the project *GREAT 2020* are:

- *Avio Aero*, a *GE Aviation* business, leader in design, manufacturing and maintenance of civil and military aeronautical components. Avio Aero is the excellence reference for the entire GE world as far as concerned the mechanical transmissions and the low pressure turbines. The headquarter is set in

Torino, that leads to a deep interaction with the Politecnico, and it counts, in addition, the plants in Pomigliano d'Arco (NA), Brindisi and Poland. From 2012 it is a GE business.

- *Politecnico di Torino*, prestigious technical university that recalls the best students worldwide, contributes to project *GREAT 2020* through the Department of Mechanical and Aerospace Engineering, Applied Science and Technology, Energy; moreover, in the campus of the Politecnico, since 2008, raises the *Great Lab*, a research pole of Avio Aero.
- *ISTEC-CNR*, the Turin unit of the Istituto di Scienza e Tecnologia dei materiali Ceramici, that pursuits research studies on ceramic materials; as far as the *GREAT 2020* is concerned the institute conducted a work aiming to define eco-friendly manufacturing processes for aeronautical alloys.
- A number of companies, such as ACTUA and EXEMPLAR, leading in advanced design and manufacturing, but also in material science and mechatronics.

In Piedmont, there are many others laboratories financed to study and improve the architecture of the aeronautical propulsion systems, that represent the success of the project *GREAT 2020*:

- *Lift Lab*, for light structures made of innovative materials.
- *Aereonflux Lab*, for high efficiency and low noise technologies for turbines.
- *Ageades Lab*, for transmission systems of new generation.
- *Zec Lab*, for low emission combustion systems.
- *MC Lab*, for aero engine mechatronic systems.

- *ECOPRO Lab*, for eco-friendly plants.



1.2 Thesis overview

The subject at the basis of this thesis project concerns the vibration mechanics of the low pressure turbines of the aeronautical engines. More specifically, the work aims to define a new simulation method that allows to perform, through a semi automatic procedure, modal analysis of blade profiles; the final goal is the development of a tool - *PRIME*, see chapter 7 - that can manage an aerodynamic input to generate a CAD, i.e. the geometry of the blade, import it into a Finite Elements Analysis environment and perform the full analysis and get as output the Campbell diagram and input files for flutter analysis. To do this, it is required to run the models into a new workspace, *ANSYS Workbench*, in place of the more traditional *Nastran*, where the entire Avio Aero legacy is built in. At the end, it is expected to get a very user-friendly multidisciplinary software that allows to manipulate complex models and results in quite simple way, leading the next generation designer throughout the process.

Two main steps have been performed:

1. The validation of a new procedure in WB to run the modal analysis for the blade profiles of the LPT stages, by comparing the results with equivalent and verified Nastran models, with very particular interest in the different contact models for the *bladed disc*, see the paragraph 6.3 for more details.
2. The validation of the same procedure for the single vane through the new tool, see chapter 7.

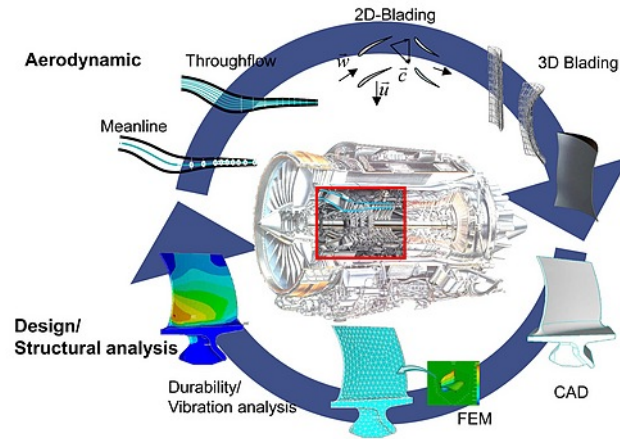


Figure 1.2.1: Design workflow of a blade profile

The automatic CAD generation is managed by a GUI internally developed in Avio Aero, *DynBooster* which allows to design, first, the airfoil profile from aerodynamic inputs, that consist in a number of 2D cross sections and the evolution from the hub to the tip; then, the geometry is completed with the hooks for the connection to the housing: beside the validation of the semi-automatic FEA process, parametric templates (see paragraph 7.1) are developed for automatic and easy handling of the CAD. The tool has been, then, uploaded into PRIME giving the possibility to manage a profile for modal analysis and fast aeromechanic assessment.

To complete the overview, it must be stressed that the results and the particular elements under investigation are property of Avio Aero, so, it will be referred to not specifying any absolute number or engine.

Chapter 2

The aeronautical engine

Before the description of the thesis, it is required to put light on the basics of the aeronautical engine, in order to lead the less skilled user to the full comprehension of the subject.

2.1 Main architectures in service

Beside particular applications, three are the major solutions in act for the civil aeronautics and all represent an evolution of the *Tutbojet*. This configuration, no more in service, took a relevant position with respect to the other endothermic engines thanks to high efficiency level: the airflow is, first, compressed and, then, burnt in the combustor in order to get a high enthalpy content fluid; finally, the thrust is given by the expansion through the turbine where the flow is accelerated and the variation of momentum generates the force that sustains the flight.

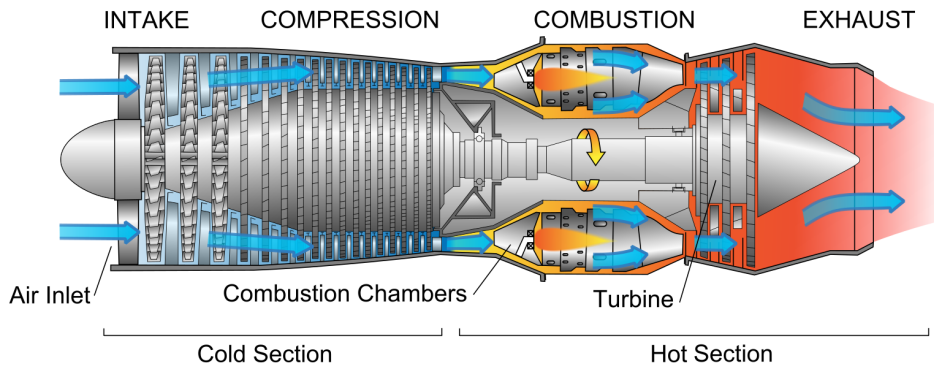


Figure 2.1.1: Turbojet architecture

2.1.1 Turbofan

The Turbofan configuration differs from the T-jet since a fan is installed at inlet. This solution allows to split the airflow into two parts: the *core* (hot flow) is sucked by the compressor and crosses the engine as described for a Turbojet; the outer section (cold flow), indeed, is not processed and does not participate to the combustion. This way, higher efficiency is achieved thanks to high speed outflow and less consumption.

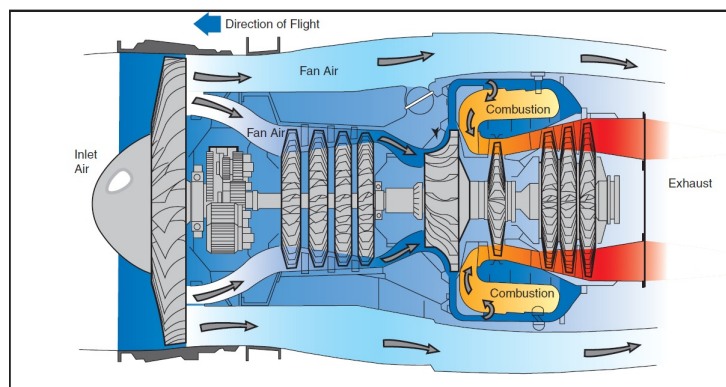


Figure 2.1.2: Turbofan architecture

2.1.2 Turboprop

From a conceptual point of view, the Turboprop follows the idea of the Turbofan by inserting a rotor at the inlet to process a greater airflow rate and, so, reduce the fuel consumption; the main difference is in the dimension of the propeller, much greater than the fan. On the other end, this represents also a limit, because at the same rotational speed, the higher the radius the higher the tangential speed: this condition falls soon in sonic chocking, destroying the efficiency. It comes out the necessity to speed down the engine and, consequently, the aircraft cruise: the turboprop, thus, is suitable for solutions where efficiency - and fuel consumption - is the major constraint.

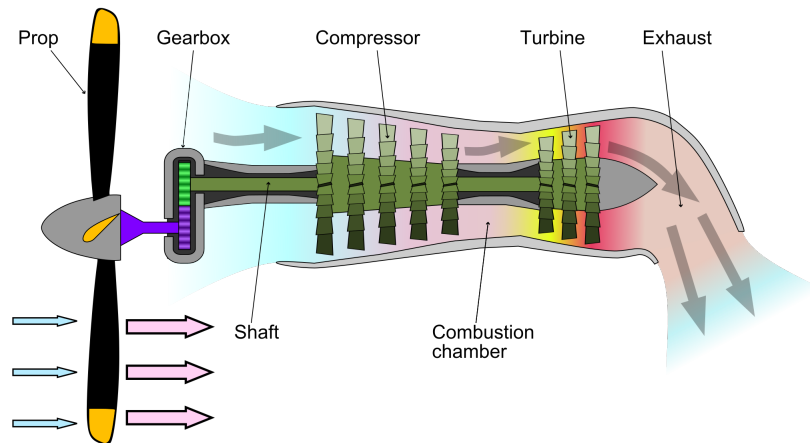


Figure 2.1.3: Turboprop architecture

2.1.3 Turboshaft

The Turboshaft is, essentially, a Turboprop configuration where the propeller is transversely mounted with respect to the engine. This is a solution for those applications which require high power output, high reliability and low weight: one example is the helicopter.

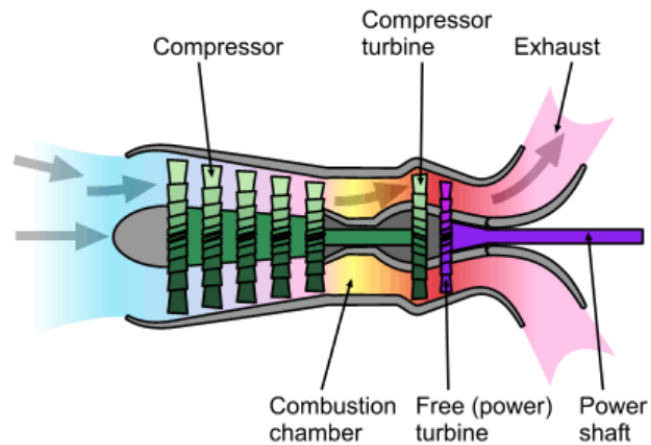


Figure 2.1.4: Turboshaft architecture

2.2 Low Pressure Turbine

The thesis work concerns the preliminary design process of LPT stages, so it is worth to explore more in detail these components. Avio Aero takes a relevant position for design and manufacturing of low pressure turbine parts which are implemented in GE Aviation engines.

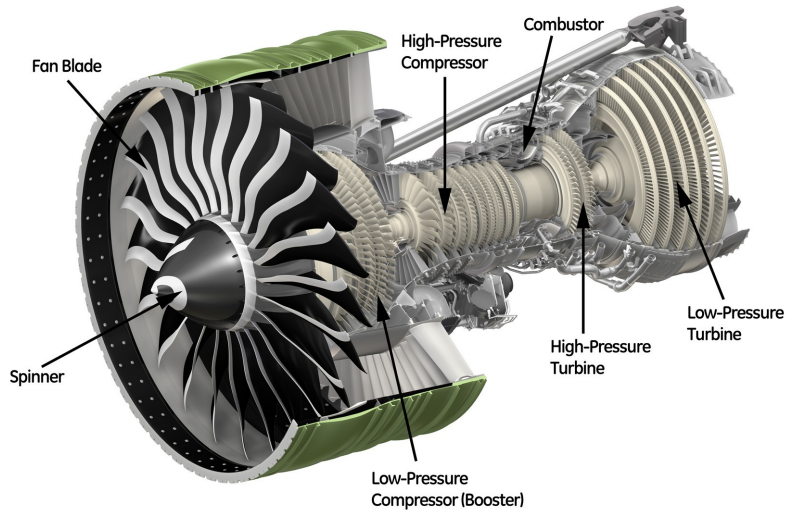


Figure 2.2.1: GE90 architecture, double shaft turbofan engine

With reference to figure 2.2.1, the GE Aviation engines are built in double-shaft configuration, meaning that one shaft connects the high pressure compressor and turbine, i.e. HPC and HPT, respectively, and a second transmission is for fan and low pressure compressor and turbine, i.e. LPC and LPT. The high pressure shaft is hollow, since it works as housing for the low pressure one. The low pressure turbine is the element with the higher power output, so, it represent the main driver for the compression stages.

The expansion cannot be performed in an unique step, therefore, the machine is subdivided in several stages, each of them defined by a *stator* - the vanes that do not rotate - and a *rotor*, fixed to the shaft in order to drag it and move the compressor.

2.2.1 LPT row

The stage of the turbine is subdivided into stator and rotor. By following the First Principle of Thermodynamics, the energy content of the fluid flow must keep constant alongside the transformation so, the expansion induces an acceleration of

the stream; high mass flow rate at high speed defines the thrust which allows to fly on.

In a very simple way, the vane profile can be assumed to be a fully constrained beam subjected to a distributed load, since it is integral to the case; it is shaped in order to lead the flow towards the inlet of the rotor stage. It is generally manufactured in segments of 3 ÷ 6 profiles, as shown in figure 2.2.2.

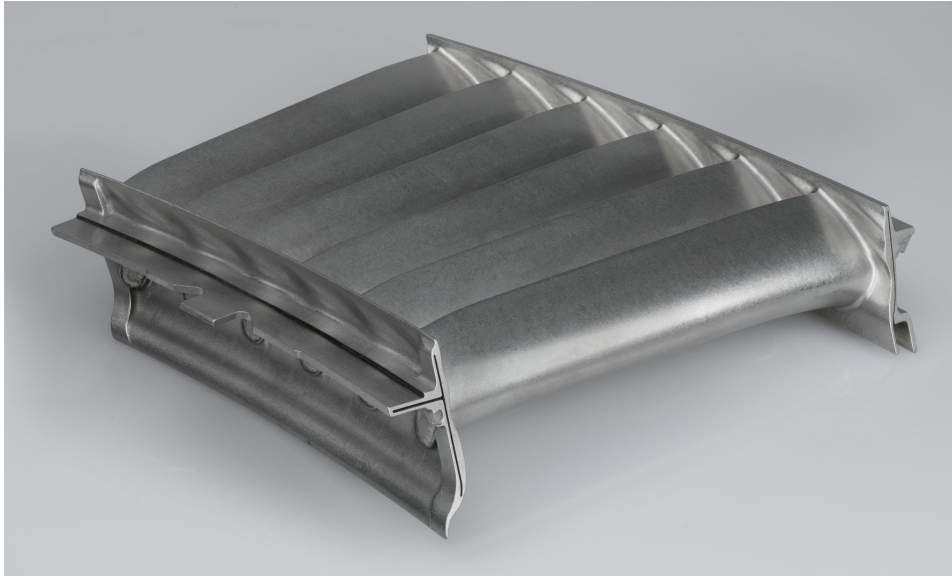


Figure 2.2.2: Vane segment

On the contrary, to scheme the rotor blade it is not straightforward: at the hub it is constrained because of the connection to the disc; at the tip the profiles are generally interlocked, meaning the blades are stocked in a rail; the aerodynamic force acts on the blade as for the vane, moreover, since it rotates about the machine axis it is affected by a centrifugal stress that can be thought as a lumped force in the center of gravity. This constraint imposes a critical design for disc and blade to avoid the concentration of mechanical stresses which induce the failure.



Figure 2.2.3: Rotor blade on the left, tip shroud enlargement on the right

To model the rotor stage for vibration mechanics analyses is not straightforward, because of the contact interaction at the tip level, red enlightenment with reference to figure 2.2.3. In general, one should consider a *stiffness* and *damping* to simulate the contact, but this would lead to a very complex model; moreover, the computational time exponentially raises. To simplify the analysis, but keeping consistency, the contact modeling does not consider any damping and the rotor is run in cyclic symmetry: the hypothesis is that the single sector is perfectly replicated alongside the 360° angle of the row by imposing appropriate coupling conditions at the contact faces.

Chapter 3

Dynamics and aeromechanics concepts for LPT

The *International Organization for Standardization*, i.e. ISO, defines the rotor as a body suspended through a set of cylindrical hinges or bearings that allow it to rotate freely about an axis fixed in the space. Despite this sentence, there are many cases in which a body behaves like a rotor but it is not constrained by any bearings: one over all is the example of the celestial bodies.

As far as this study is concerned, the rotor is that part of the machine which rotates about the central line of the engine and interacts with the airflow, the *bladed disc*. Because of the interaction with the fluid - at high pressure and temperature - from one side, and the centrifugal stress on the other, the system is mainly subjected to quasi-static loads; by the way, they are *dynamic* inputs, so, they induce mechanic vibrations. Now, depending on the characteristics of the model, they come out several conditions where the amplitude of the oscillation is maximum, so, the resistance of the body is minimum. This condition is called *resonance* and represents that moment in which the body cannot sustain the excitation, the energy content raises and, finally, fails.

The simplest example to clarify the concept is the failure of the Tacoma bridge in November 1940 when the excitation induced by the wind flow made the structure to fall in resonance until the break.



Figure 3.0.1: Failure of Tacoma bridge

The Tacoma is not an example of rotor, but it shows the relevance of dynamic analyses in prediction of the failure conditions.

The stage of a turbine is made, as already explained, by a stator and a rotor. The first leads the stream towards the rotor blades in order to limit the losses for poor contact of the fluid to the wall and, beside, performs a little expansion; the latter interacts with the fluid to rotate and convert the majority of the energy content into mechanical work that is, then, available to the shaft.

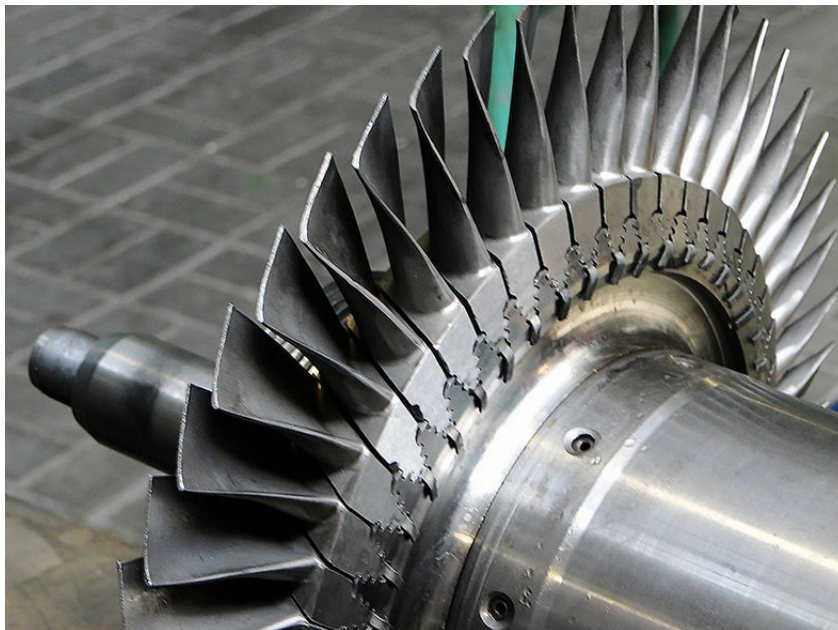


Figure 3.0.2: Example of bladed disc mounted on the shaft

The disc cannot uncouple the blade, since, depending on its stiffness, it influences somehow the behavior of the rotor. To be coherent, thus, between the bodies might be considered a contact and they cannot be studied as a unique entity, i.e. *blisc*, blade and disc represent one body.

3.1 Excitation on the bladed disc

The issues induced by the mechanical vibrations in a bladed disc are:

- Efficiency loss of the energy conversion.
- Crack generation in the structure, so the failure.

Due to these criticisms, the engine have to be designed in order to avoid extended working conditions where the dangerous vibratory phenomena might rise.

The branch of vibration mechanics concerning the turbomachinery falls into the *aeroelasticity*: by definition, it is the interaction of inertial, elastic and aerodynamic phenomena on a structure hit by a fluid flow. The output vibrations represent, thus, a design threshold for the engine.

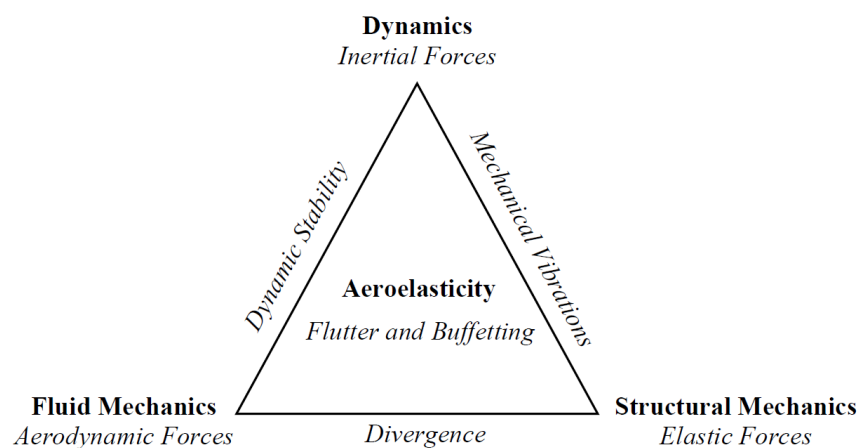


Figure 3.1.1: Triangle of the aeroelasticity

If the interaction does not consider the inertial contribute the aeroelasticity is *static*; on the other way, the *dynamic aeroelasticity* is a multidisciplinary subject, where the most relevant cases are the *forced response* and the *flutter*.

3.1.1 The forced response

The forced response investigates the forces of the fluid flow on the structure deriving from the external disturbs of the neighboring rows with respect to the one under study. The purpose is to avoid resonance conditions, i.e. the external load behaves close to a natural frequency of the system.

Both, the stator and rotor are defined by a number of profiles equally spaced alongside the 360°; this means the interaction fluid/structure is harmonic, i.e. it periodically repeats in each sector, so, the outcoming load is periodic.

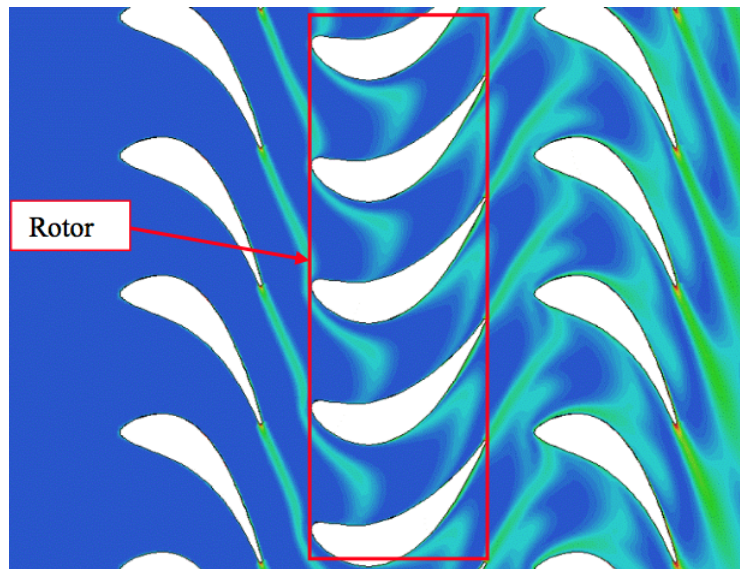


Figure 3.1.2: Interaction of the stator and rotor stage

The rotational speed of the rotor and the number of the blades of the row drive the *fundamental frequency* of the force. The other harmonic contributes are integer multiples of the fundamental one and depend, the same way, on the engine

rpm and the number of blades and are defined through the *Engine Order*. The Engine Order is the ratio between the frequency of the force and the rotational speed of the row.

The excitation, thus, is associated to a frequency which depends on the rotation of the disc; to enlighten possible resonance points, the Campbell diagram is most suitable tool.

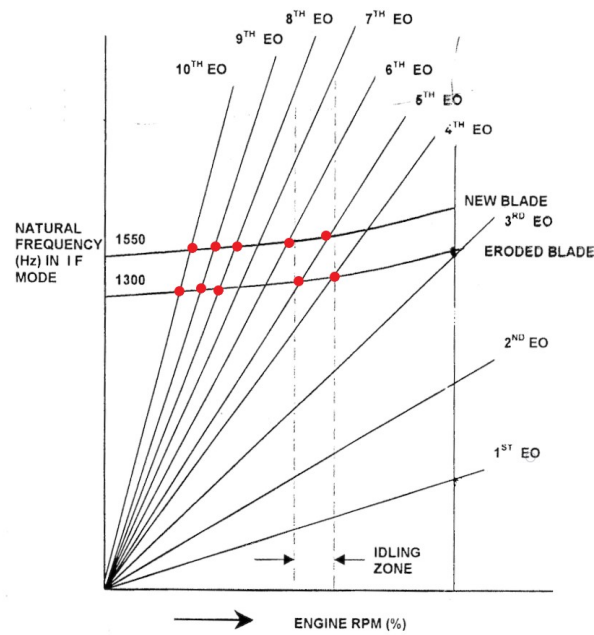


Figure 3.1.3: Example of Campbell diagram

With reference to figure 3.1.3, a resonance condition appears once the frequency of the external force coincides with the natural frequency of the rotor, as shown by the red spots.

3.1.2 Flutter

As already anticipated, the interaction fluid/structure can drive to oscillations deriving from the coupling of aerodynamic, elastic and inertial forces. No external loads is counted into: the deformation of the structure under the aerodynamic

forces influences the load in return and so on; the resulting pulsating phenomenon can fall into instability.

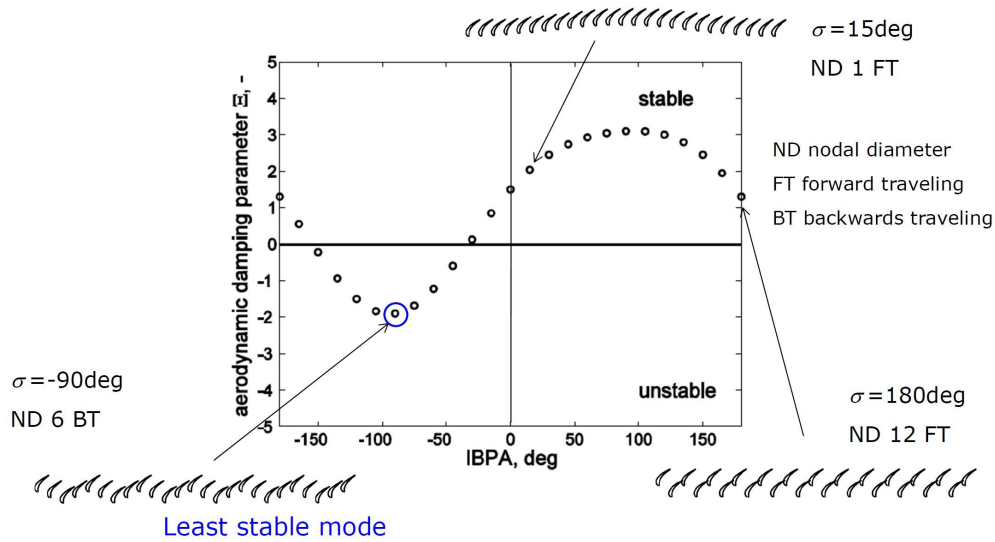


Figure 3.1.4: Example of aeroplots, below the 0 damping is negative, thus, the system is unstable

The energy of the system grows at each cycle and the oscillation amplitude cannot be controlled: sooner, the blade fails due to crack propagation or fatigue.

The flutter check, as will be explained better in chapter 5, is evaluated only when the geometry of the blade is frozen for manufacturing; if the flutter analysis shows instability, the profile can be only modified *a posteriori*. The idea sustained in this thesis project to define a Aero-Mech design for LPT to process more detailed analyses, such as the flutter check, at preliminary stage is, thus, very consistent.

3.2 Modal analysis

The modal analysis is at the basis of mechanical studies. It concerns the definition of the vibratory behavior of a system; the results is a set of *natural frequencies* and associated *modeshapes*.

To clarify better the concept, it is proposed below the example of a simple multi degrees of freedom system: it represents a *structure*, i.e. no phenomena related to rotation.

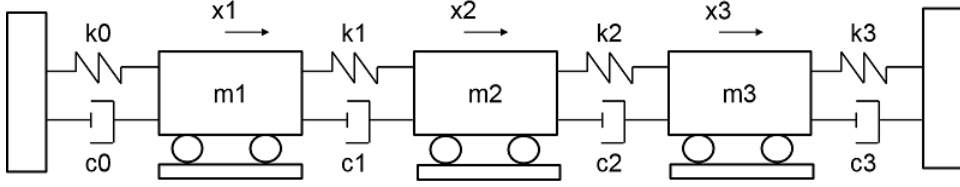


Figure 3.2.1: Example of multi degrees of freedom system

A body, in general, is defined by mass, damping and stiffness properties. In the simplest example of a *linear system* the three characteristics might be distinguished and treated separately, as shown in fig. 3.2.1. The system is made by three masses (m_1, m_2, m_3) free to move only in the horizontal direction (x_1, x_2, x_3); the connection to the walls and the other masses is defined by stiffness, k_i , and damping, c_i . Any mass is associated to one displacement, being three bodies, the system counts three degrees of freedom.

Saying that $F(t)$ is the generic excitation to the system, the *equation of motion*, i.e. eom, can be written as:

$$[m]\{\ddot{x}\} + [c]\{\dot{x}\} + [k]\{x\} = F(t) \quad (3.1)$$

where $[m]$, $[c]$, $[k]$ are, respectively, the mass, damping and stiffness matrix $n \times n$, $\{x\}$ is the dof vector $n \times 1$ and $\{\dot{x}\}$ and $\{\ddot{x}\}$ are the velocity and acceleration vector. n is the number of dof: in this case three.

The solution to the system can be written as the sum of a *general integral* and a *particular integral*; the first one depends on the characteristics of the system, i.e. mass, damping and stiffness, the latter is the system response to the particular input $F(t)$. Aiming to simplify the expression to ease the solution, the $[c]$ matrix is generally neglected and damping taken into account downstream.

The *free response*, or the general integral, is the solution to the unforced system, i.e. no input; this problem is described as *eigenproblem* and can be written as:

$$([k] - \omega^2[m])\{\psi\} = \{0\} \quad (3.2)$$

where ω_i^2 are the *eigenvalues* and $\{\psi\}_i$ are the *eigenvectors* of the system; the couple $(\omega^2, \{\psi\})$ represents the modeshape at the natural frequency:

$$f_n = \frac{\sqrt{\omega^2}}{2\pi} \quad [Hz] \quad (3.3)$$

The forced response depends, on the other end, on the particular input.

As result, the complete response of the system will be the *superimposition* of the two integrals.

3.2.1 Modeshapes of a bladed disc

A bladed disc is a rotating system, so, the modal analysis might consider this aspect.

The disc can be seen, in first approximation, as a set of identical sectors on the 360°; this allows to run the modal analysis by employing the cyclic symmetry (see chapter 4 for more details) to simplify the model and reduce the computational time. In this case, the modeshapes are characterized by particular *nodal diameters* or *nodal circles*; they represent lines and circles where, for a given mode, the vibration amplitude of the structure is null.

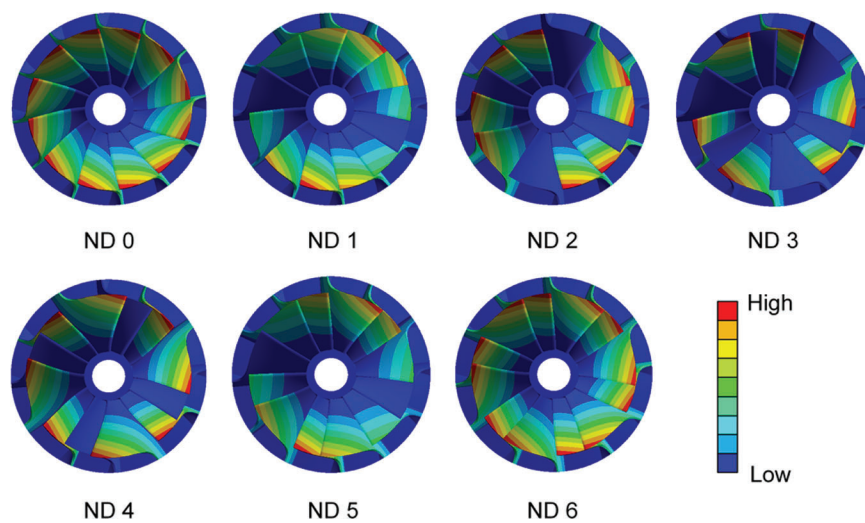


Figure 3.2.2: Example of a 12 blades rotor modeshapes

The number of nodal diameters which can be seen on a bladed disc depends on the number of blades, or sectors; said N the set of profiles, it comes out:

$$0 \leq n \leq \frac{N}{2} \text{ if } N \text{ even}$$

$$0 \leq n \leq \frac{N-1}{2} \text{ if } N \text{ odd}$$

Depending on the nodal diameter under analysis, the resultant vibratory behavior can be of two different kinds:

- *Static modeshapes*, the modal displacements of any sector are equal in amplitude and phase and the eigenvector (see eq. 3.2) is a real entity. This is verified when the modes count a nodal diameter 0 or $\frac{N}{2}$, with N even.
- *Rotating modeshapes*, it is for any other nodal diameter; the vibration can be described by a couple of forward and backward *traveling wave* with respect to the rotational speed. This way, any sector is out of phase (ϕ) than the neighboring ones; the mode is defined by a couple of *modal* orthogonal eigenvectors.

Given the eigenvector of one rotating mode, it is straightforward to compute the second one, since the orthogonality property.

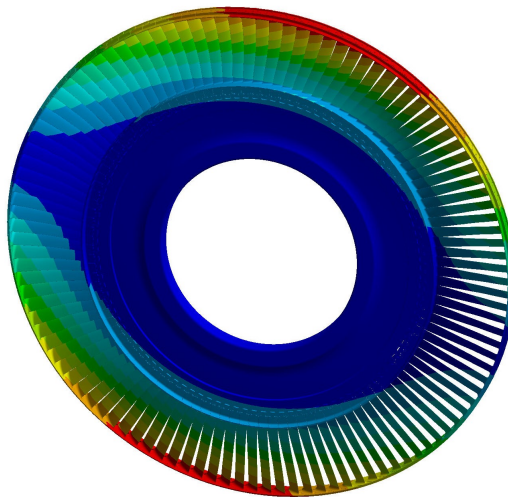


Figure 3.2.3: Bladed disc, Nodal Diameter 1, forward wave

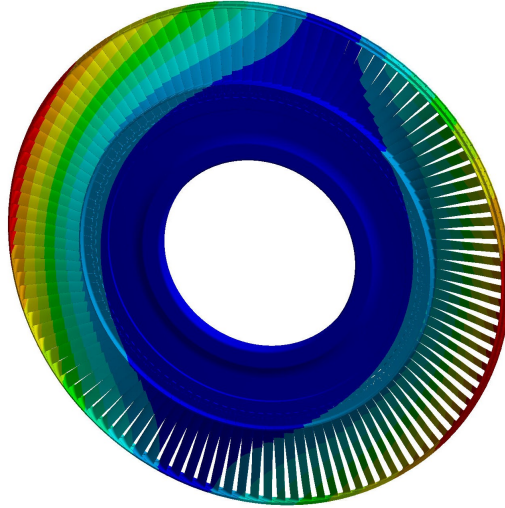


Figure 3.2.4: Bladed disc, Nodal Diameter 1, backward wave

The fig. 3.2.3 and 3.2.4 show a forward and backward rotating mode, respectively, of a bladed disc which counts 112 profiles for nodal diameter 1; the phase of each sector ϕ is function of the nodal diameter and the length of the row; it is defined as the *Interblade Phase Angle*, i.e. IBPA, as:

$$IBPA = \frac{2\pi}{N}n \quad (3.4)$$

where N is the number of blades and n the nodal diameter.

The eq. 3.4 defines the modal displacement of each sector: in this case, two following blades vibrate the same way, but a phase shift ϕ .

The IBPA, as the nodal diameter, describes the modeshapes of a rotating system.

3.2.2 Different modal shape families

For any *real* dynamic system, the modeshapes are infinite in number, thus, the natural frequencies. In a rotating system, the eigenfunctions are related to the nodal diameters, but the approach keeps the same: for any configuration there are an infinite number of eigenvalues. In case of a FEM, Finite Element Model, where

the system is split into a *finite* number of dof, the modes are limited in number. It is possible, so, to determine a modal *family* associated to any given modeshape. The classification of the families might be easily plotted on the *FreND* diagram, i.e. Frequency Nodal Diameter, as shown in fig. 3.2.5.

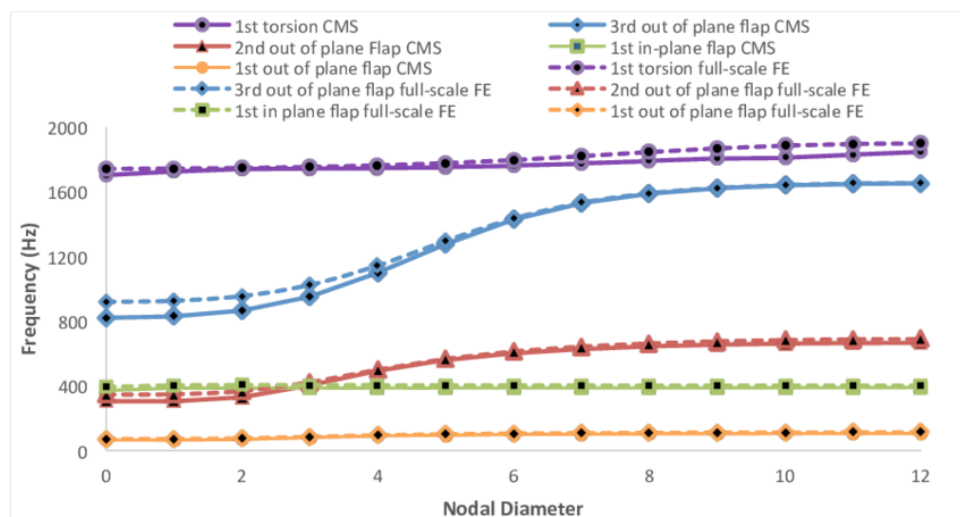


Figure 3.2.5: Example of FreND diagram

In fig. 3.2.5 is reported the trend of each mode with respect to the nodal diameter: the natural frequency tends to increase up to a given ND, not equal for any mode, and then approach to an asymptote. The lower diameters, where the frequency grows, represent the vibratory modes of the disc: in this configuration the blade does not deform; on the contrary, for a high diameter, the frequency approaches to an asymptote showing the modes related to the blade, i.e. the disc behaves extremely rigidly. The *blade modes* represent a similar vibratory behavior of the airfoil for different nodal diameters.

The principal modal behaviors of the blade are:

- *Edgewise*, i.e. EW.
- *Flapwise*, i.e. FW.
- *Bending*, i.e. 1F.

- *Torsion*, i.e. 1T.

To better explain, the modeshapes concerning the deformation of the blade are reported as follow.

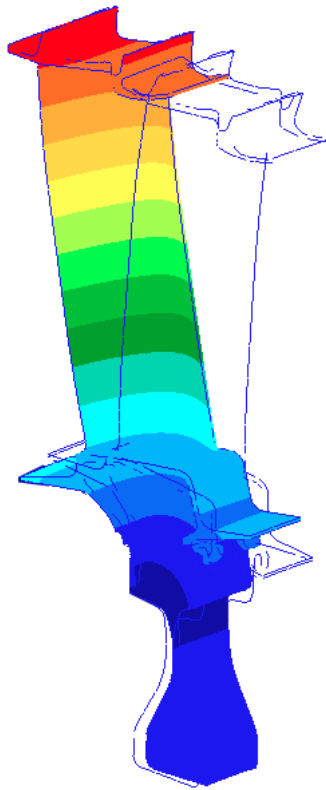


Figure 3.2.6: Edgewise

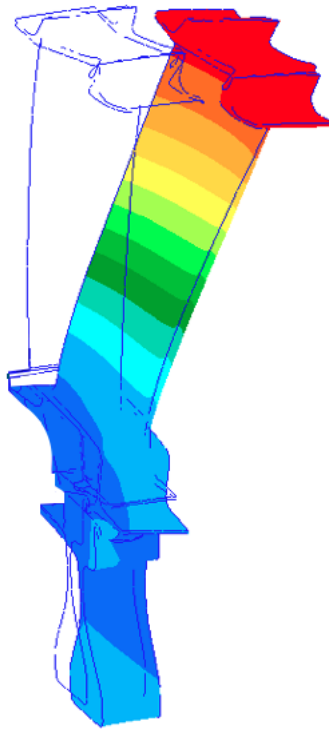


Figure 3.2.7: Flapwise

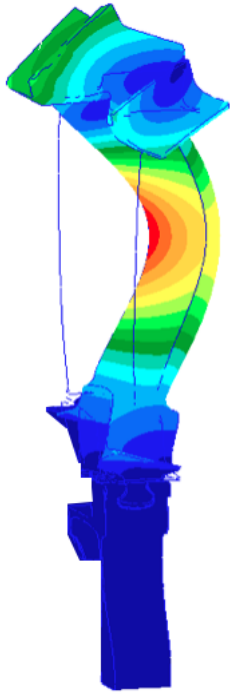


Figure 3.2.8: Bending

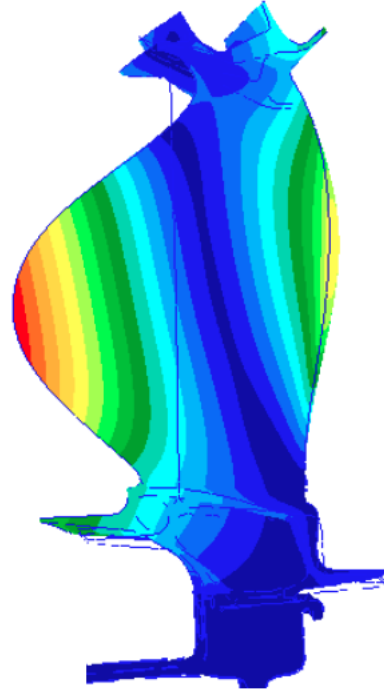


Figure 3.2.9: Torsion

3.2.3 Campbell diagram

Since the Campbell diagram is one of the desired output of the proposed semi-automatic process it is worth to spend more details about it.

This plot is one of the most important means to investigate the instability of a rotating system due to its own velocity. Strictly speaking, on the ordinates they are reported the *modeshapes* of the rotor, i.e. the natural frequencies function of the rotation Ω ; on the abscissa the excitation to the system. When the diagram enlightens a *crossing*, i.e. the intersection of a natural frequency and a forcing, the rotor falls, potentially, into instability.

At the inlet of the rotor stage, even in steady state condition, the pressure

signal is not coincident with the mean value, but shows fluctuations induced by disturbing elements, such as bearings, gaskets, vanes. From here, it depends a periodic force on the blades which, by following the *Fourier Transform*, can be seen as the sum of a number of harmonic inputs. The excitation frequency depends of the revolution of the body in the form:

$$f = \frac{n \Omega}{60} \quad [Hz] \quad (3.5)$$

where Ω is the rotational speed of the engine and n is the *Engine Order*.

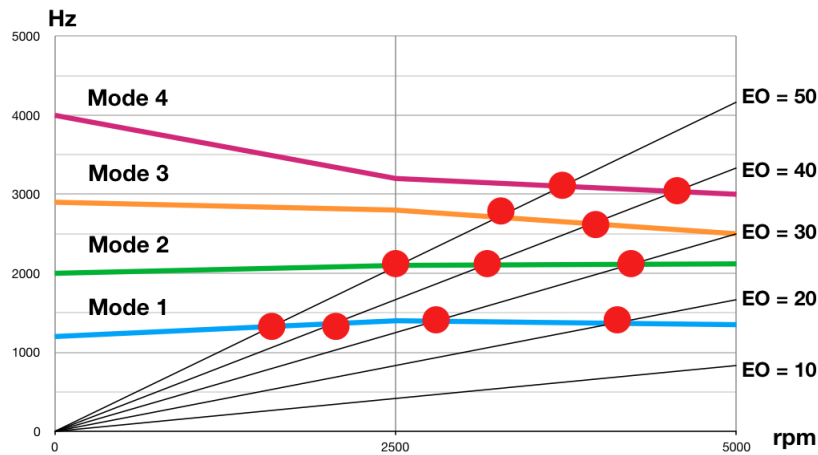


Figure 3.2.10: Example of Campbell diagram: crossings EO/modeshapes are potentially resonance conditions

The modeshapes derive from the modal analysis: not being a structure, it is reasonable to experience a variation of the frequencies against the rotational speed; there are three main causes:

- *Centrifugal load*, the rotational speed induces a stiffening on the blade.
- *Thermal load*, the temperature distribution alters the material properties, as the Young modulus and Shear modulus.
- The *Gyroscopic effect*.

Beside the modeshapes, the second set of curves in the diagram represents the Engine Orders, concerning the forcing function.

The red spots in fig. 3.2.10 show possible resonance conditions, i.e. the forcing function behaves with the same natural frequency of the crossed mode at a given rotational speed. It is not straightforward the resonance points fall into dangerous vibration; this is mainly for:

- The forcing amplitude might have low intensity.
- The aerodynamic and structural damping can be sufficient to control the vibration.
- For high Engine Orders the vibration amplitude is low.

As shown, the Campbell diagram is a powerful tool to investigate potential vibratory issues at a given rotational speed. In the standard design workflow, this is a *detailed* result generated downstream the casting release for manufacturing, i.e. once the geometry of the blade is frozen. In case of crossing points in the working speed range, the only possibility to fix them is by local modifications of the geometry; this means the production costs rise and not the optimal profiles is employed.

By means of a robust and semi-automatic process which allows to quickly iterate the preliminary mechanical design downstream the optimization of the aerodynamic profile, the Campbell diagram might be generated straightforward showing eventually inconvenient crossing; thus, the blade profile can be opportunely modified and, then, checked in few minutes.

3.2.4 Modal Assurance Criterion

In experimental modal analysis, the modeshapes of a system might be studied by *exciting* the body with an *impulsive input*. The structure is, firstly, setup

with proper accelerometers, i.e. instruments that allow to investigate the local acceleration of the body; then, by means of an *instrumented hammer*, the system is excited and starts to vibrate.

By manipulating the output signal, it is possible to build the modeshapes of the system for any selected natural frequency.

The same system might be, on the other hand, modeled in a finite element software and modal analysis run. To appreciate to goodness of the model, the eigenvectors of experimental and numerical analysis can be compared to enlighten any correlation.

To this purpose, the most employed parameter is the *MAC*, i.e. *Modal Assurance Criterion*, which states 1 when the eigenvectors represent the same mode, 0 otherwise.

$$MAC = \frac{|\{\Psi_T\}^T \{\Psi_S\}^*|^2}{(\{\Psi_T\}^T \{\Psi_T\}^*)(\{\Psi_S\}^T \{\Psi_S\}^*)} \quad (3.6)$$

where the subscripts T and S state, respectively, the numerical and experimental eigenvector, the superscript T means *transpose*, i.e. the vector $n \times 1$ is written as $1 \times n$, where n the number of dof, the superscript $*$ means *complex conjugate*, i.e. the imaginary part of the entity is multiplied by 1.

In reality, because of the numerical errors, the eq. 3.6 does not strictly give the unit when the modes correspond and zero when they are dissimilar. In general, if the MAC is lower than $0.6 \div 0.7$ the modeshapes are probably different, while if the result is next to 1 they might be correspondent eigenvectors.

In this thesis work, the numerical modeshapes have not been compared with experimental data, but, for validation of modal analysis approach in Ansys Workbench (see chapter 6) with respect to Nastran results, the MAC has been employed.

Chapter 4

Rotors in cyclic symmetry

The blade is a quite complex model to be investigated. The modal analysis described in paragraph 3.2 might be run, for a rotor, by means of advantageous symmetry properties; this approach is suitable once the hypothesis that the body is made on a number of identical sectors along the 360° is done. In reality, the imperfections coming from the manufacturing induce blades which are not identical; by the way, to investigate the behavior at the preliminary level, the *cyclic symmetry* is a huge tool to be employed in order to reduce the computational time.

By recalling the eq. 3.1, the modal analysis derives from the solution of the eigenproblem expressed by the eq. 3.2:

$$([k] - \omega^2[m])\{\psi\} = \{0\} \quad (3.2)$$

where the number of extracted eigenmodes, (ω_i^2, ψ_i) , corresponds to the degrees of freedom of the body.

The cyclic symmetry approach consists in modeling one sector of the entire row and running the modal analysis once the body has been opportunely constrained; in fact, by extracting one bladed disc from the whole structure, it is possible to enlighten couples of interfaces: here, it is requested to formulate *coupling* equations in order to derive the displacements of the neighboring blades from the basic sector, i.e. the one under analysis.

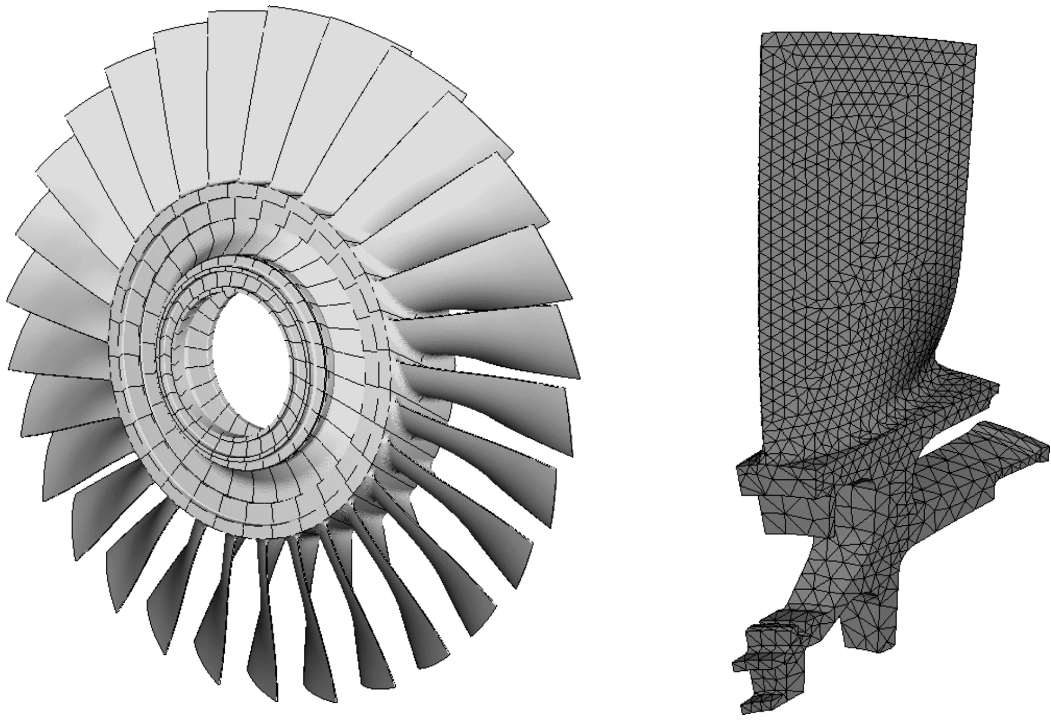
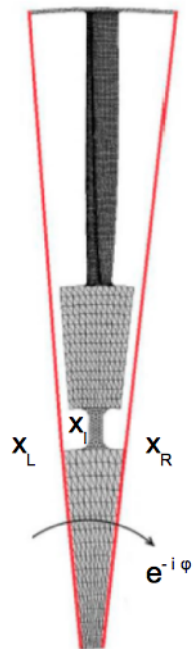


Figure 4.0.1: Bladed disc row and single sector



$$\begin{bmatrix} x_R^A \\ x_R^B \end{bmatrix} = \begin{bmatrix} \cos(k\alpha) & -\sin(k\alpha) \\ \cos(k\alpha) & -\sin(k\alpha) \end{bmatrix} \begin{bmatrix} x_L^A \\ x_L^B \end{bmatrix} \quad (4.1)$$

Figure 4.0.2: Cyclic interfaces of the bladed disc

With reference to fig. 4.0.2 and eq. 4.1:

- $k = \text{Harmonic Index}$ ranges in between $\left[0, 1, 2, \dots, \frac{N}{2}\right]$ if N is even, in between $\left[0, 1, 2, \dots, \frac{N-1}{2}\right]$ if N is odd; N is the integer number of sectors.
- α , is the pitch angle, i.e. $\frac{2\pi}{N}$.
- x represents the dof vector, displacements and rotations.
- x_L^A represents the basic sector, i.e. A , left side.
- x_R^A represents the basic sector, i.e. A , right side.
- x_L^B represents the duplicated sector, i.e. B , left side.
- x_R^B represents the duplicated sector, i.e. B , right side.

The vector of the degrees of freedom of the basic sector (see fig. 4.0.2) might be arranged in order to put in evidence the variables concerning the cyclic symmetry, as follows:

$$\begin{bmatrix} x^s \end{bmatrix} = \begin{bmatrix} x_L^s \\ x_I^s \\ x_R^s \end{bmatrix} \quad (4.2)$$

The eq. 4.2 states the separation of the dof in three groups:

1. Left, L , are the interface dof on the left side of the sector.
2. Inner, I , are the inner dof of the sector.
3. Right, R , are the interface dof on the right side of the sector.

The vector has dimension $n \times 1$, if n is the total number of dof of the sector; to properly run the analysis, the nodes of the grid on the interfaces might be identical, i.e. the associated 2D meshes equal.

With the same approach, the forcing vector can be written the same way.

$$\begin{bmatrix} F \end{bmatrix} = \begin{bmatrix} F_L \\ F_I \\ F_R \end{bmatrix} \quad (4.3)$$

Recalling the eq. 3.2, the equation of motion to be solved becomes:

$$([k^s] - \omega^2[m^s])\{x^s\} = \{F\} \quad (4.4)$$

The angular offset between the sectors is taken into account through the eq. 4.1; in compact form:

$$\{x_R^s\} = e^{i\phi}\{x_L^s\} \quad (4.5)$$

where the angle ϕ corresponds to $k\alpha$. The set of dof becomes, thus:

$$\begin{bmatrix} x^s \end{bmatrix} = \begin{bmatrix} x_L^s \\ x_I^s \\ e^{i\phi}\{x_L^s\} \end{bmatrix} \quad (4.6)$$

The eq. 4.6 states the number of unknowns (for the complete system $2n + N$) decreases up to $n - N$, where n defines the dof at the interfaces and N the remaining ones.

The cyclic symmetry approach allows to clarify better the concept of rotating and static modeshapes. The eq. 4.5 might be further manipulated:

$$\{x_R^s\} = e^{i\phi}\{x_L^s\} = \{x_L^s\} \left(\cos\left(\frac{2\pi n}{N}\right) + i \sin\left(\frac{2\pi n}{N}\right) \right) \quad (4.7)$$

where $\phi = \frac{2\pi n}{N}$, n the nodal diameter and N the number of blades. For $n = \left[0; \frac{N}{2}\right]$ the phase is, respectively, 0 and π , thus, the solution is real; otherwise, the imaginary part is different than 0. The natural frequencies for $0 \leq \phi \leq \pi$ and $\pi \leq \phi \leq 2\pi$ are equal in absolute value, but associated to opposite traveling waves.

The final equation for modal analysis solution in cyclic symmetry is, then:

$$([k^s](\phi) - \omega^2[m^s](\phi)) \begin{bmatrix} x_L^s \\ x_I^s \end{bmatrix} = [0] \quad (4.8)$$

which is conceptually equivalent to the expression 3.2, but the dof are manipulated in order to enlighten the parameters of the cyclic symmetry and the mass and stiffness of the sector are functions of the phase angle ϕ : fixed the phase, the solution is computed and modes extracted. The total number of modeshapes that might be computed for a *N-bladed disc* is:

- If N is even, the modes are $\frac{N}{2} + 1$: $\phi = \left[0, \alpha, 2\alpha, \dots, \left(\frac{N}{2} - 1\right)\alpha, \pi\right]$
- If N is odd, the modes are $\frac{N + 1}{2}$: $\phi = \left[0, \alpha, 2\alpha, \dots, (N - 1)\alpha\right]$

where $\alpha = \frac{2\pi}{N}$ is the pitch angle of the basic sector.

Chapter 5

The design of LPT stage

The design of a new turbine stage is a quite complex procedure which is the result of two different studies: from one side the *aerodynamics* is focused on performance and optimization of the fluid energy conversion into mechanical work; on the other one the *structural mechanics* that studies the resistance of each component to mechanical stress and defines the limit life of the engine. Since the interaction fluid/structure, it is required, in addition, the *aeromechanic* check to investigate potentially unstable working points where the vibratory behavior of the blades is sustained by the airflow; for that reason, downstream the structural analyses, flutter investigations are run.

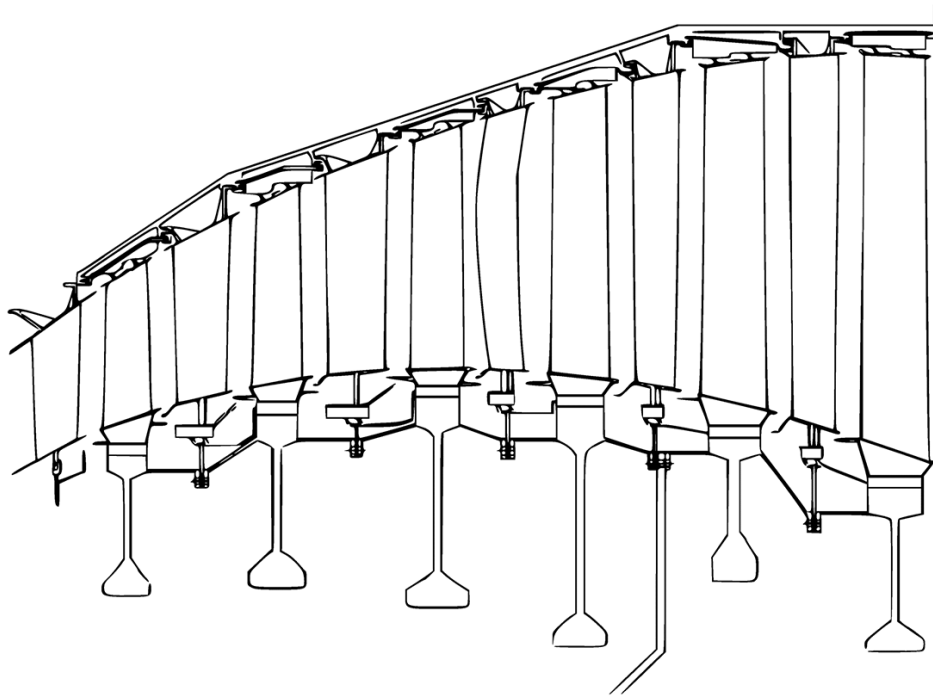


Figure 5.0.1: LPT cross section

The preliminary design of the LPT is preceded by the conceptual study of the whole engine from the point of view of performance. The goal is to define:

- Broad measures of the engine.
- Rough cross section based on global inlet/outlet pressure drop.
- Power output.

Then, the corner points are further elaborated in order to define pressure drop and massflow rate of each component of the system. As far as this work is concerned, the focus will be on the *Low Pressure Turbine*.

5.1 The aerodynamic design

The goal is to determine the profile of the blade that better processes the thermodynamic transformation to obtain the target output.

The aerodynamic design is subdivided into three main steps:

1. *1D optimization process*: on the basis of the boundaries coming from the conceptual design, the turbine is split in stages and each one further subdivided into a potential number of sectors; then, depending on the thermodynamic evolution to be performed in each stage, they are defined boundary constraints for the airfoils, such as the leading and trailing angle and the trend of the profile from the hub to the tip for the velocity triangles sketch (i.e. the fluid path through the machine), the endwall and the rotational speed to process the required massflow rate.

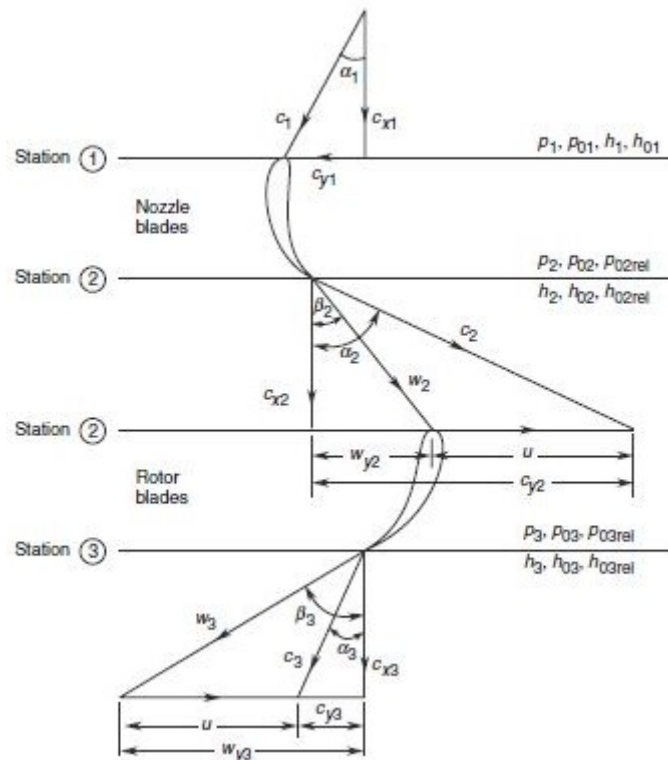


Figure 5.1.1: Velocity triangles for a turbine stage

2. *Base 3D profile*: through a number of empirical correlations coming from the Avio Aero know-how, the outcomes of the 1D design are elaborated in order to obtain the 3D shape that answers the best the performance requirements; at this level, the CFD, *Computational Fluid Dynamics*, on multi-rows (i.e. all the stages involved) configuration is run to determine the response of the turbine. Moreover, this result will be employed for BCs setting for the next optimization loop.

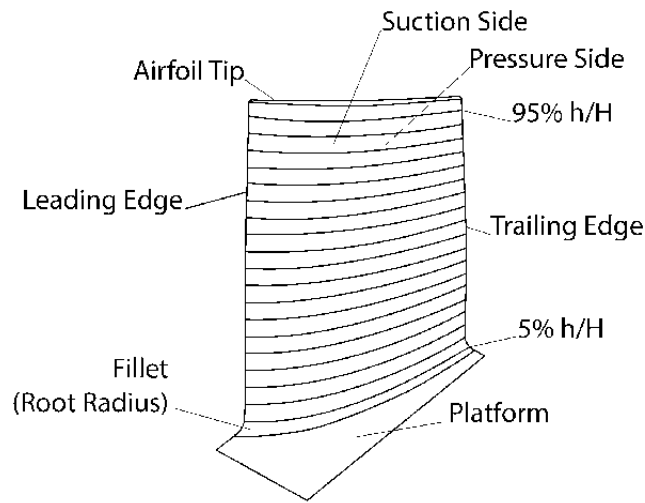


Figure 5.1.2: Airfoil nomenclature

3. *Optimization*: among all the investigated shapes, the ones that respect the BCs and success the fluid dynamic analyses are frozen for detailed design; the geometry is investigated in terms of leading and trailing edge, chordal length (i.e. the axial extension of the blade), thickness distribution. The variation range is limited in few percentage points and, then, the performance trend is plotted: if the configuration leads to an increase of the outcome with respect to the base profile it is frozen as *Aero Pass* and available for mechanical analysts for structural check.

5.2 The preliminary mechanical design

Before starting the mechanical assessment, the aerodynamic profile needs boundaries for inner and outer band, so it is handled first by a CAD designer.

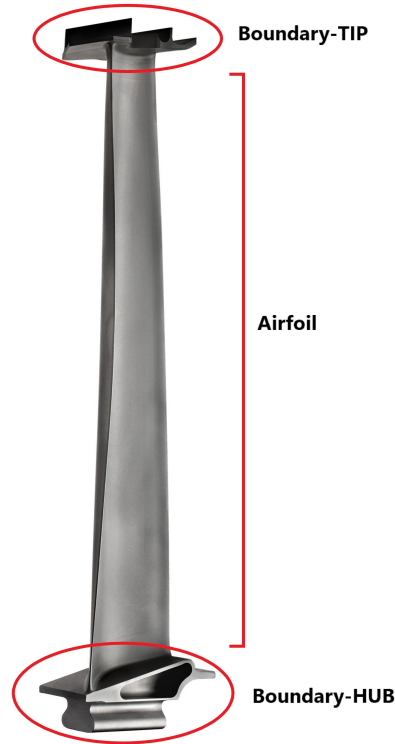


Figure 5.2.1: Boundaries of the airfoil

Once the geometry is completed, the blade is verified from mechanical point of view: this part concerns the generation of a Finite Elements Model, *discretization* of the part into volumes and nodes aiming to simulate the dynamic behavior of the body. Therefore, two main results are needed at this level: from one side the *free response* of the system, especially to investigate the robustness of different contact models between the blades, on the other the *static deformation* due to the pressure field and the centrifugal load coming from the rotation about the machine axis, in order to evaluate the mechanical stresses in steady state condition.

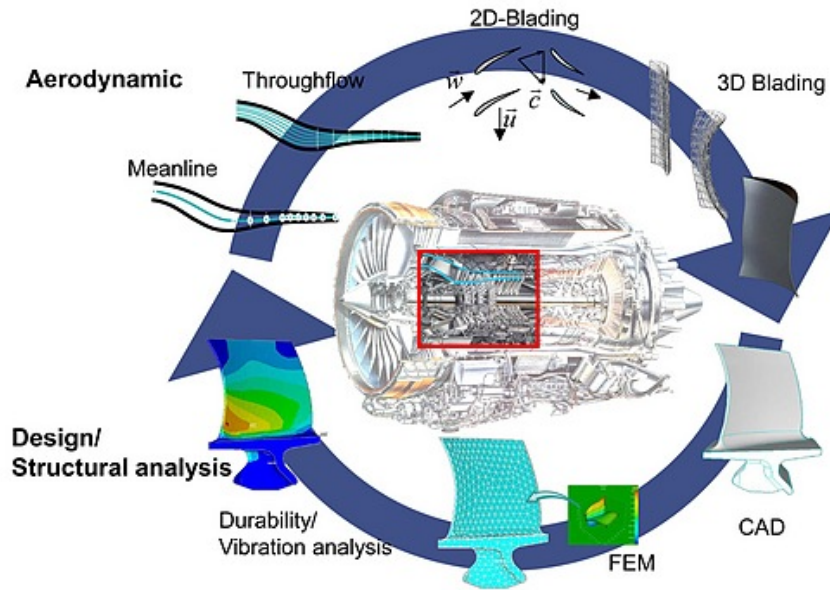


Figure 5.2.2: Design workflow of a blade profile

If the analysis gives not good results, the profile is sent back to Aero team for further investigation and the process is reiterated, otherwise the geometry is *frozen* for next design stage.

The detailed design concerns more specific studies, such as the generation of Campbell diagrams to evaluate the response of the engine throughout the speed range, and the check to flutter, i.e. instability of the blade due to interaction with fluid-flow. If the check is positive, the geometry is definitively frozen for casting.

The crucial point of the workflow is that, once the geometry is consolidated for manufacturing, other detailed analyses are further run to define the *fatigue limit*; so, if the safety factors are not verified the only way to improve the behavior is by local modifications or *fixing*.

It means that the profile that goes in service is not the *global optimus*, but it is a blade deriving from two distinguished optimization loops; if limits come out, they are locally treated without considering a general overview of the process.

5.3 The Aero-Mech design concept

What represents the best choice from one side can lead to issues on the other: this drives to errors and mismatching because a general and complete overview of the process misses; the proposal of this thesis work is, thus, to formulate a model for *Aero-Mech* design, where the two spheres merge and optimization loops concern the targets of both at the same time. First, by anticipating at preliminary level more detailed analyses, then by looking to mechanical thresholds too at blade profile generation level.

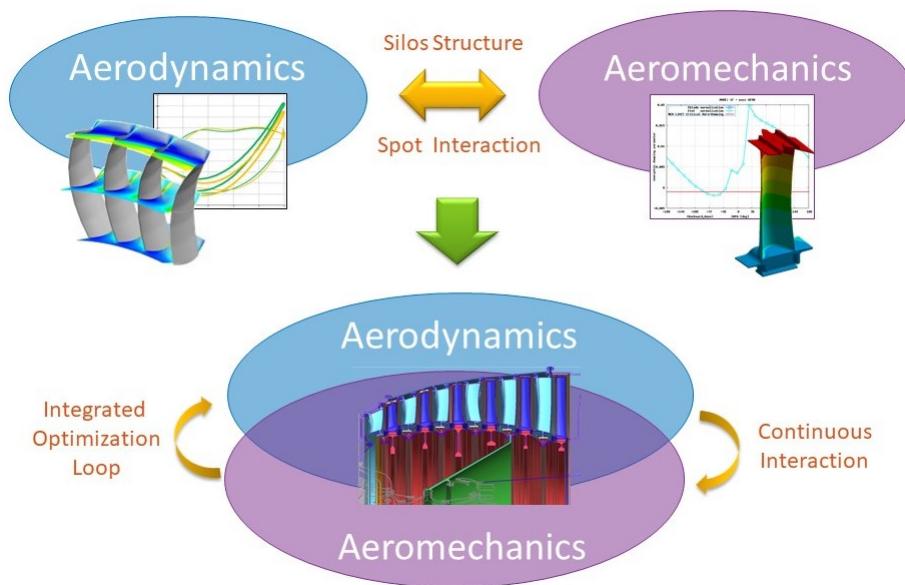


Figure 5.3.1: Aero-Mech optimization

Following this approach, it will be possible in the future to need a new design figure, being familiar with the whole science behind the process and being able to understand the *all* analysis results and so make proper decisions.

The tool *PRIME* -**P**reliminary **aeR**omechanics **I**ntegrated **M**ultidisciplinary **E**nvironment - has been developed with the idea to make the preliminary design more robust in order to:

- Give to aerodynamics the confidence with mechanical feedback in easy way,

so modify the profile of the blade not only looking to performance but also mechanical resistance; the *Aero* designer can iterate *in the loop* structural analyses to optimize the shape during its generation.

- Automate the process from the CAD generation to the modal analysis solution and automatically evaluate the Campbell diagram; more detailed assessments might be run in advance without any additional costs, since the overall computational time is deeply reduced.
- Link together different workflows in one unique process, by reducing time costs and sources of errors.

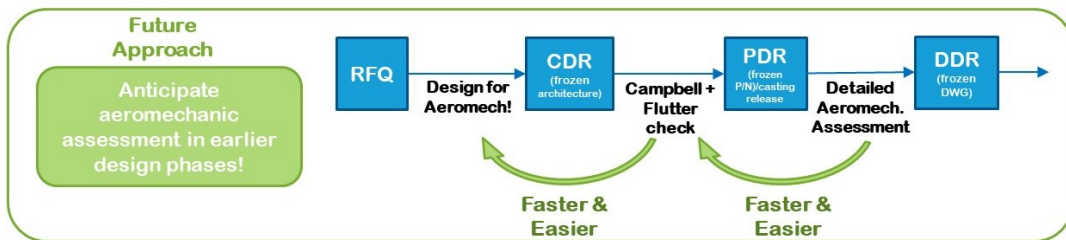


Figure 5.3.2: Design process improvement with the tool PRIME

The drastic reduction of the computational time and, so, the possibility to anticipate more detailed analyses, lead to freeze an *optimized* geometry, that means less fixings and global design costs.

5.3.1 *PRIME* overview

The construction of the tool has been possible thanks to the benefits occurred once the Finite Elements Analysis is run in Ansys Workbench; in this environment,

the model can be set-up in more easy and robust way because it is possible to make use of interesting features to automate the process. It is a very important point to stress, since at preliminary level it is required to figure out the *goodness* of the profile from both aerodynamic and mechanic point of view; the generation of the FEM in this phase is a standard procedure, so the automation through a parametric approach represents a reasonable decision.

The followed approach for designing PRIME is described below:

1. Automatic CAD profile generation from Aero input through the 2D cross sections at specific radii, from the hub to the tip;
2. Adaptation of parametric templates (i.e. consistent CAD for the boundaries of the profile generated by following a parametric approach for scaling) for inner and outer band scaled with respect to a reference length of the profile;
3. Semi-automatic modal analysis in WB to point out the free response of the body in order to plot the Campbell diagram and screen the behavior throughout the speed range of the engine.

Even if the concept is very easy to understand, the tool construction is not straightforward: the first model taken into account is the vane stage, since it can be represented as constrained-constrained beam thermally loaded.

The whole Avio Aero legacy concerning aeromechanic analysis for LPT has been for years in the MSC Nastran environment, so at the beginning the validation of the analogous procedures in WB workspace has been conducted; besides, it has been investigated the setting of the best workflow to iterate the model and post-process the results in the new tool.

The final goal of this study is the implementation of the real rotor geometry, i.e. the bladed disc; with this idea, the validation and optimization of the modeling procedure in WB has been conducted also for this configuration, where the cyclic

symmetry is involved.

Chapter 6

Validation of *Workbench* procedure

The software *MSC Nastran* and *Ansys Workbench* are mainly employed for Finite Elements Analysis, or FEA. The body is divided into a number of regions, called *finite elements*, whose deformation is described by means of nodes; the deformed shape of each finite element is assumed to be a linear combination of a set of functions of space coordinates through a certain number of parameters, considered as the degrees of freedom of the element.

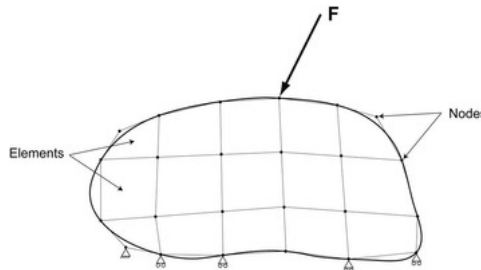


Figure 6.0.1: Finite Element Model example

Strictly speaking, the SW Nastran lets to the user large degree of freedom in setting up the model but, on the other way, it needs high skills to pass through all features. The final result is a text file containing all the information concerning the FEM that the solver reads to compute the solution: this means that the model can be modified *by hand*, but it is not straightforward. High number of degrees of freedom in defining the model does not allow to automate a process in a robust way.

On the other hand, WB is *easier* to use because it is based on geometrical

features, such as faces and volumes; moreover, meshing part can be automated thanks to predefined functions that adapt the grid size, i.e. the dimension of the elements, on the specified target, face or 3D body.

Modeling time is strongly reduced and the possibility to reiterate the procedure by means of an optimization loop decreases the chance of error.

6.1 Vane

The vane model is the easiest to setup because it is mainly equivalent to a simple beam constrained at the ends. It represents the stator of the stage, so no centrifugal load is applied; moreover, not requiring the cyclic symmetry, the mass and stiffness matrix are *real*, i.e. they do not contain complex entries, so the solution to the eigenproblem is real.



Figure 6.1.1: Vane profile of LPT

The lower and upper part that bound the profile are, respectively, the *Inner Band* and *Outer Band*. They represent the elements through which the profiles are put in contact to each other to form the whole row. To be more precise, it should be noted that the vane is manufactured by segments which group three up to six elements (see fig. 2.2.2), but for simplification purposes, the analyzed model contains only one profile (as shown in figure 6.1.1).

The faces of OB and IB (Outer Band and Inner Band) supposed to be in contact with the neighboring profiles are, in this case, grounded. This means that the displacements of the nodes are set to zero in all three directions (*SPC*, or Single Point Constraints).

Then, a radial temperature distribution is associated to all grid nodes.

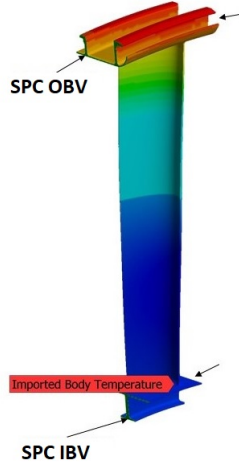


Figure 6.1.2: Boundaries and thermal load on Vane stage

The solution to the eigenproblem comes from an iterative approach: in order to be sure to apply the same algorithm as Nastran, the solver, that generally is automatically selected by the SW depending on the particular model, must be forced on *Direct* mode. This setting means that the solution algorithm selected is *Block Lanczos*. The latter, indeed, has been identified as the most similar to the one used by Nastran for the various test cases considered.

To be consistent, the comparison is valid by working on the same grid: it has been employed an existing and verified bdf Nastran file (i.e. the file generated downstream the model setting), then imported into WB. Then, the BCs are setup and the computation run as described above.

Of course, for the same reason just explained, the same material properties are used in both workspaces.

The frequency variation is, then, computed as relative percentage error of the solution calculated in WB with respect to the Nastran one by means of the formulation:

$$\epsilon = \frac{|f_N - f_{WB}|}{f_N} \cdot 100 \text{ [%]} \quad (6.1)$$

where f_N is the frequency of Nastran model and f_{WB} the WB one.

<i>Mode</i>	ϵ [%]
1	0.01
2	0.05
3	0.06

Table 6.1: Relative error on frequency base between Nastran and WB model - vane

The results show a percentage error lower than 1% validating the new procedure in WB: by following this approach, the free response of the vane sector is in accordance with the equivalent model run in Nastran.

In addition, to be more confident on matching, the MAC has been verified (see paragraph 3.2.4): the analysis showed a unitary value for the corresponding mode-shapes, as supposed by the theory, by assuring the correlation between the two different solutions.



Figure 6.1.3: 1F

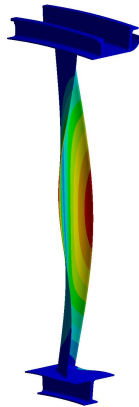


Figure 6.1.4: 1T

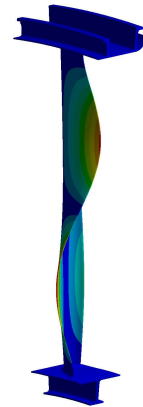


Figure 6.1.5: 2F

With reference to paragraph 3.2.2, the first two figures represent the bending and torsion; the figure 6.1.5 represents the second bending mode, since it shows a rest point in the middle of the airfoil.

6.2 Simplified Blade

As far as the rotor stage is concerned, the bladed disc, i.e. blade and disc, is the most representative model, but it is, for that, complex to study because there are two bodies and cyclic symmetry is involved. To simplify, simulation is run by investigating the *blade only* configuration, aiming to consistently replicate the BCs at the contact surfaces at the dovetail (the region in contact to the disc), by reducing the complexity and the computational time.

The simplified blade, or blade only, is modeled mainly as the vane apart two aspects:

1. The centrifugal stiffening induced by the rotation is considered, so the eigenproblem is solved starting from a *prestressed* configuration;
2. The contact at the tip shroud may assume different formulations, i.e. tight interlocking, radial free interlocking, tip free and single point.

With reference to figure 6.2.1, the lower part of the profile is subdivided into the *shank*, i.e. the hollowed part with the extensions, and the *dovetail*, the bottom end that connects the blade to the disc. The upper part is the *tip shroud*, where it is enlightened the contact surface between the airfoils, i.e. the interlocking face.

The modeling is in line with the one described for the nozzle. At the dovetail level, the surfaces that are in contact with the disc are grounded - no nodal displacements -, while at the interlocking the condition can be of different types.

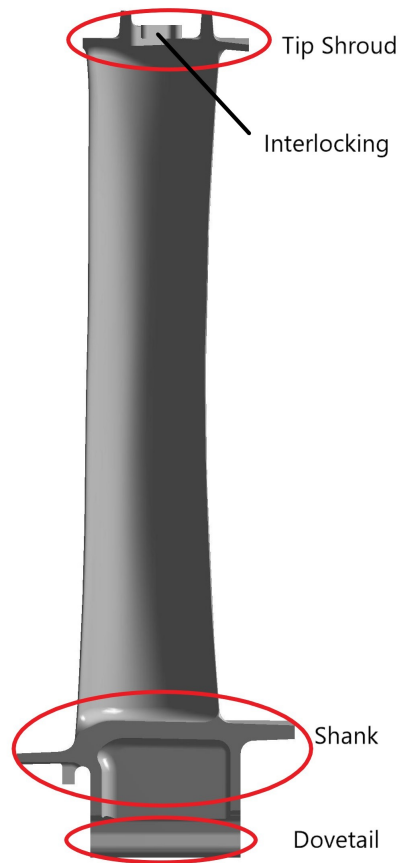


Figure 6.2.1: Blade profile of LPT

The possible contact configurations are:

- *Tight interlocking.*
- *Radial free interlocking.*
- *Single Point.*
- *Tip free.*

Of course, depending of the contact model, the system stiffness changes; for the tight condition the beam is fully locked, so the resultant model will be more rigid and the free vibrations higher. On the other end, the tip free configuration is approximately equivalent to a constrained-free beam and so the resultant stiffness

will be the lowest one.

The contact model which shows the most consistency is the radial free: for that, the blade only has been studied in this configuration.

Being a rotor stage, it is applied a centrifugal load by means of the definition of the rotational speed. To properly model the contact at the shroud, the grid nodes have been transformed into the cylindrical frame, by employing the feature *Nodal Orientation*; expressing the nodes with respect to r , θ , z , it is straightforward to keep free the radial component.

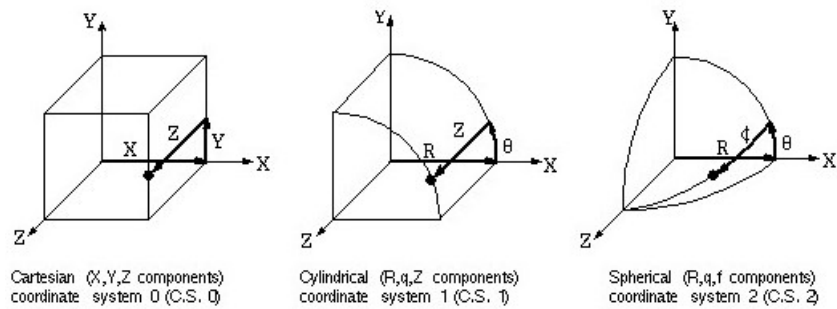


Figure 6.2.2: Cartesian, cylindrical and spherical frame in Ansys Workbench

As for the vane, material properties are kept constant and the same mesh employed in order to compare same model and properties. By looking to the first six modeshapes, the results are showed in table 6.2:

<i>Mode</i>	ϵ [%]
1	0.15
2	0.12
3	0.05
4	0.00
5	0.16
6	0.03

Table 6.2: Relative error on frequency base between Nastran and WB model - blade only

The error is computed by means of the 6.1 and, again, by setting the solver *Direct* the delta is deeply lower than the 1%: the simplified model run in WB is consistent with Nastran.

The MAC number has been verified for this configuration too and gave positive result.

6.3 Bladed disc

The complete rotor stage is formed by a disc and an airfoil, i.e. bladed disc; the disc allows the connection between the blade and the power shaft (see fig 3.0.2). To run the modal analysis on the entire row is very time and memory consuming even for a high performance calculator; for that reason, it is common use to follow the theory of the traveling wave that concerns, in terms of model setting, the application of a cyclic symmetry constraint. This way, the computational time is deeply reduced with respect the full model and the result are, anyhow, robust if compared with experimental ones.

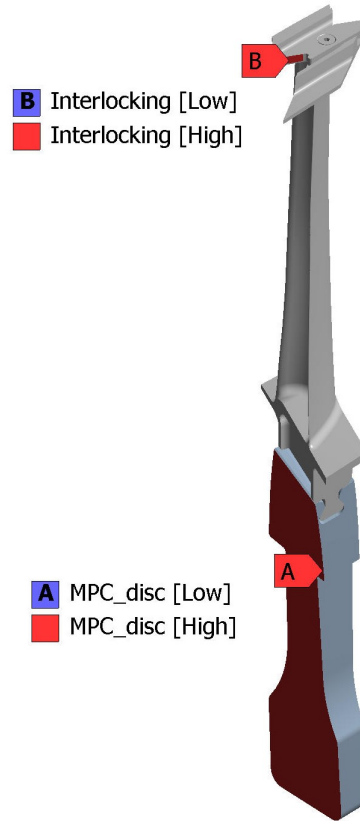


Figure 6.3.1: Bladed disc profile of LPT with cyclic symmetry constraint

With reference to fig. 6.3.1 the cyclic symmetry is set at two different interfaces:

1. At disc pressure/suction side by coupling the three dofs.
2. At the interlocking region: here, the constraining depends on the particular contact model that is supposed to simulate.

The definition of the cyclic constraint is very intuitive in WB through the GUI: once a proper cylindrical reference frame is created, it is enough to select the involved surfaces and the axis of rotation. To apply this condition it is essential that the 2D meshes of the faces to be coupled are identical.

It must be stressed, anyway, this approach works until at the disc and tip shroud the same contact model is considered; in fact, radial free and single point configuration

are taken into account through few *APDL Mechanical* command lines. APDL is the primitive Ansys solver for FEA and it is, actually, recalled in background to compute the solution for this kind of models.

The key is the command *cyclic* through which it is possible to force the constraint between nodes and not only faces: so, in case of single point configuration (i.e. two nodes involved in cyclic symmetry at the tip shroud) the coupling is straightforward once the corresponding grid points on pressure and suction side at interlocking are enlightened.

CYCLIC, NSector, Angle, KCN, Name, USRCOMP, USRNMAP

The number of sectors of the row and the pitch angle define the cyclic system: the first one corresponds to the number of the blades, while the second one is the angular extension of each element; it is enough to clarify one out of two since they are linked by the expression:

$$Angle = \frac{360^\circ}{NSector} \quad (6.2)$$

KCN is the ID of the cylindrical frame in which to write the coupling equations.

To pass the nodes involved in the symmetry there are two possibilities: defining groups of nodes with proper name for pressure and suction side, or defining a map of nodes paired by two. By following the first approach it is required to name the groups, or *Named Selections*, with a proper root and declare it in place of Name; while for the second one it is enough to use a default structure for the map, name it and pass the identification in place of USRNMAP.

The procedure is not straightforward if compared to the default one through the GUI, anyhow not particular skills are required.

```

USE EXISTING MODEL FOR CYCLIC SYMMETRY

*****
***** INPUT QUANTITIES *****
*****
*   NUMBER OF SECTORS =                112           *
*   CYCLIC COORDINATE SYSTEM =          1           *
*   COMPONENT NAME ROOT =          CYCLIC           *
*   USER EDGE COMP PAIR COUNT =         2           *
*   LOW  EDGE COMPONENT = CYCLIC_M01L           MATCHED *
*   HIGH EDGE COMPONENT = CYCLIC_M01H           *
*   LOW  EDGE COMPONENT = CYCLIC_M02L           MATCHED *
*   HIGH EDGE COMPONENT = CYCLIC_M02H           *
*****

```

Figure 6.3.2: Extract solution log file, cyclic symmetry correctly set

Here, again, the comparing is performed with respect to a validated Nastran model, run for different contact configurations, in order to import the corresponding bdf file into WB and work on the same grid.

For the bladed disc, two bodies are involved in the model: at the contact region is imposed a Multi Point Constraint, so no sliding and detach are taken into account between them.

Then, in the bottom region of the disc is set a rolling BC, in order to simulate the contact with the neighboring stage.

Finally, the setup of centrifugal and thermal load is the same as vane and simplified blade: the prestressed configuration, starting point for modal analysis, is, thus, computed.

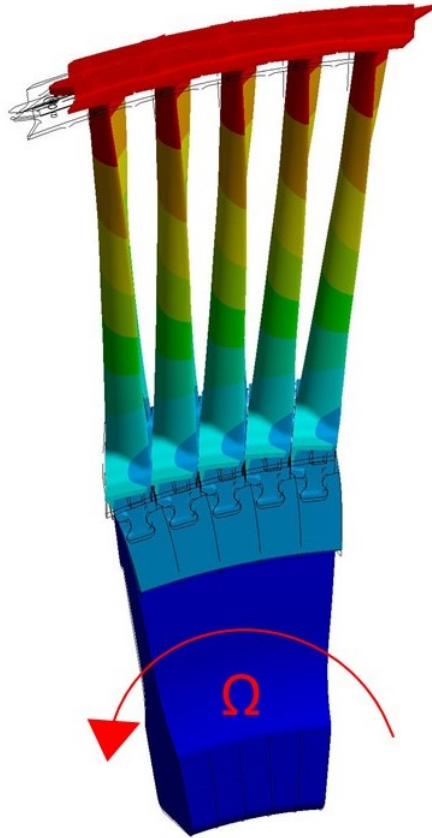


Figure 6.3.3: Bladed disc under centrifugal load

Since the bladed disc gives complex modeshapes, the setup of the eigenproblem passes through the definition of the *harmonics* by means of the command *cyclopt*:

CYCOPT, Hindex, Value1, Value2, Value3

that allows to run the harmonic indexes from *Value1* to *Value2* by step *Value3*; by repeating the command a proper number of times, all the desired harmonics can be computed.

If the cyclic symmetry is correctly setup, WB is able to rebuild the entire row, possibly to appreciate the traveling wave running.

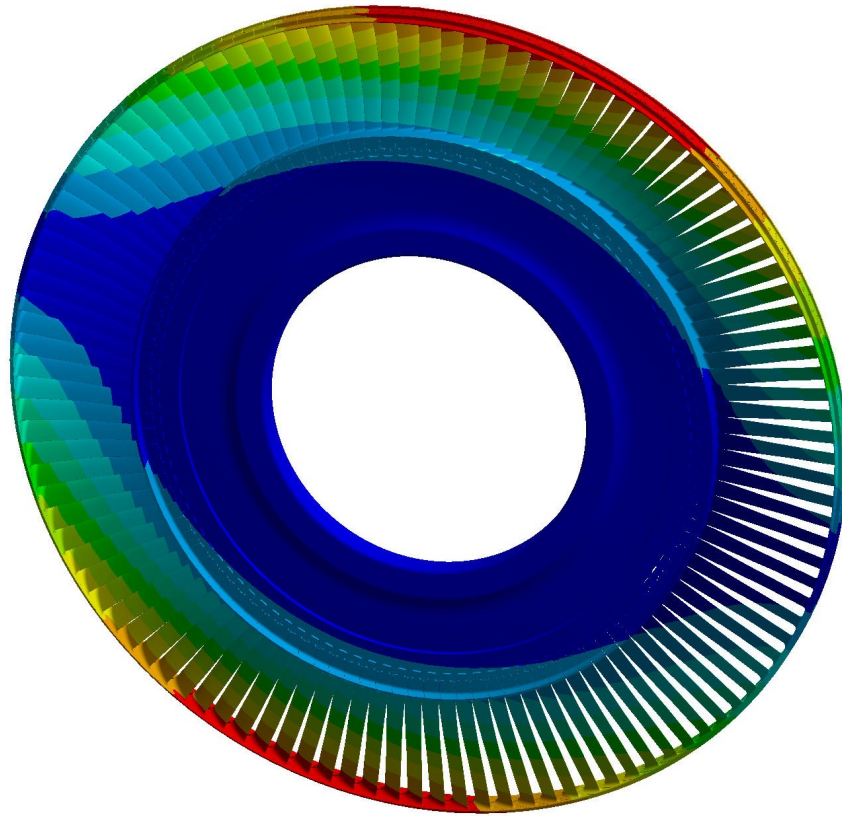


Figure 6.3.4: Traveling wave on bladed disc row

6.3.1 Tight Interlocking

With the tight interlocking the cyclic nodes at the tip are fully constrained as well as the ones on the disc. The stage under investigation counts 112 blades and so the studied harmonics fall in the range $[1 \div 56]$. Beside the different setup, the comparing is performed the same way as vane and simplified blade on frequency base.

<i>Harmonic</i>	<i>Mode</i>	ϵ [%]
1	1	0.55
1	2	0.14
1	3	0.67
1	4	0.07
1	5	0.25
5	1	0.02
5	2	0.19
5	3	0.51
5	4	0.25
9	1	0.40
9	2	0.09
9	3	0.02

<i>Harmonic</i>	<i>Mode</i>	ϵ [%]
14	1	0.48
14	2	0.12
14	3	0.00
19	1	0.28
19	2	0.17
19	3	0.03
23	1	0.13
23	2	0.13
28	1	0.11
28	2	0.06
33	1	0.11
33	2	0.05

<i>Harmonic</i>	<i>Mode</i>	ϵ [%]
37	1	0.11
37	2	0.07
42	1	0.11
42	2	0.07
47	1	0.11
47	2	0.08
51	1	0.11
51	2	0.09
55	1	0.11
55	2	0.09

Table 6.3: Relative error on frequency base between Nastran and WB model - blisc - Tight Interlocking

For any harmonic, so nodal diameter, it is possible to extract a number of natural frequencies, as explained in paragraph 3.2.2; as already said, for high harmonics the modes that can be studied decrease. In addition, the tight interlocking configuration is the stiffest one, so this aspect is more evident than other cases.

The resultant error is lower than 1% throughout the entire range, so the two procedures, in Nastran and WB, are equivalent.

For the bladed disc, since the complexity induced by the rotating modes shapes, the MAC has not been investigated; a further comparing between the SW has been done on the basis of the prestress: the maximum displacement due to the centrifugal load has been analyzed and the relative error showed results below the 1%. All following configurations have been investigated this way, showing all of them positive match.

6.3.2 Radial Free

Radial Free contact refers to a configuration at the tip shroud where the radial dof is kept free. The setting of the constraint is done through the command *cycopt*, but in place of *Hindex* is recalled the feature *DOF*: this way, it is possible to couple the tangential and axial displacement, keeping free the radial one.

CYCOPT, *DOF*, *Value1*, *Value2*, *Value3*, *Value4*

The grid nodes involved in cyclic symmetry must be grouped by Named Selection for the imposition of the constraint; as explained, the name has to follow a standard structure and inside the nomenclature a numerical ID is reported in order to manipulate many pairings (see fig. 6.3.2). So, in place of *Value1* is indicated the identification number of the pair, while *Value2*, *Value3* and *Value4* represent the constrained dofs; they are indicated as *ux*, *uy* and *uz* and an empty cell means unconstrained displacement. In case of cylindrical frame the nomenclature is unchanged, but the meaning is different: they express *r*, *θ* and *uz*. Finally, the first cell is empty to keep the radial dof free.

The analysis results are, thus:

<i>Harmonic</i>	<i>Mode</i>	ϵ [%]
1	1	0.55
1	2	0.11
1	3	0.47
1	4	0.33
1	5	0.01
5	1	0.02
5	2	0.07
5	3	0.70
5	4	0.26
9	1	0.41
9	2	0.16
9	3	0.01

<i>Harmonic</i>	<i>Mode</i>	ϵ [%]
14	1	0.52
14	2	0.17
14	3	0.01
19	1	0.27
19	2	0.28
19	3	0.04
23	1	0.15
23	2	0.19
23	3	0.14
28	1	0.11
28	2	0.05
33	1	0.11
33	2	0.02

<i>Harmonic</i>	<i>Mode</i>	ϵ [%]
37	1	0.10
37	2	0.02
42	1	0.09
42	2	0.01
47	1	0.09
47	2	0.01
51	1	0.09
51	2	0.01
55	1	0.08
55	2	0.09

Table 6.4: Relative error on frequency base between Nastran and WB model - blisc - Radial Free

Again, the error on frequency is lower than 1% showing the robustness of the WB model in comparing with the Nastran one.

6.3.3 Single Point

The validation of the Single Point configuration is a massive milestone of the entire benchmarking procedure, since other works conducted in Avio Aero showed that this model is the closest one to the experimental behavior; moreover, by reducing the total number of nodes involved in cyclic symmetry induces an important reduction of the calculation time.

As well as the other configurations, the Single Point shows positive results.

<i>Harmonic</i>	<i>Mode</i>	ϵ [%]	<i>Harmonic</i>	<i>Mode</i>	ϵ [%]	<i>Harmonic</i>	<i>Mode</i>	ϵ [%]
1	1	0.01	19	1	0.03	42	1	0.08
1	2	0.01	19	2	0.02	42	2	0.02
1	3	0.02	19	3	0.13	42	3	0.12
1	4	0.05						
1	5	0.13	23	1	0.04	47	1	0.08
			23	2	0.03	47	2	0.02
5	1	0.02	23	3	0.13	47	3	0.12
5	2	0.02						
5	3	0.02	28	1	0.05	51	1	0.09
5	4	0.15	28	2	0.03	51	2	0.02
			28	3	0.13	51	3	0.12
9	1	0.02						
9	2	0.01	33	1	0.06	55	1	0.09
9	3	0.11	33	2	0.03	55	2	0.02
			33	3	0.13	55	3	0.12
14	1	0.02						
14	2	0.02	37	1	0.07			
14	3	0.14	37	2	0.02			
			37	3	0.12			

Table 6.5: Relative error on frequency base between Nastran and WB model - blisc - Single Point

By observing here too an error lower than 1% throughout the investigation range, the Single Point approach in WB is, thus, validated.

6.3.4 Tip Free

The Tip Free modeling is partially analogous too the Tight Interlocking, but the tip shroud is unconstrained. The results are:

<i>Harmonic</i>	<i>Mode</i>	ϵ [%]
1	1	0.08
1	2	0.31
1	3	0.15
1	4	0.37
1	5	0.52
5	1	0.02
5	2	0.09
5	3	0.13
5	4	0.10
5	5	0.69

<i>Harmonic</i>	<i>Mode</i>	ϵ [%]
9	1	0.00
9	2	0.15
9	3	0.03
9	4	0.10
9	5	0.07
14	1	0.01
14	2	0.15
14	3	0.04
14	4	0.11
14	5	0.04

<i>Harmonic</i>	<i>Mode</i>	ϵ [%]
19	1	0.01
19	2	0.15
19	3	0.04
19	4	0.11
19	5	0.04
23	1	0.02
23	2	0.15
23	3	0.05
23	4	0.11
23	5	0.03

<i>Harmonic</i>	<i>Mode</i>	ϵ [%]
28	1	0.02
28	2	0.16
28	3	0.05
28	4	0.12
28	5	0.03
33	1	0.02
33	2	0.16
33	3	0.05
33	4	0.12
33	5	0.03
37	1	0.03
37	2	0.16
37	3	0.05
37	4	0.12
37	5	0.02

<i>Harmonic</i>	<i>Mode</i>	ϵ [%]
42	1	0.03
42	2	0.16
42	3	0.05
42	4	0.12
42	5	0.03
47	1	0.03
47	2	0.16
47	3	0.05
47	4	0.12
47	5	0.02

<i>Harmonic</i>	<i>Mode</i>	ϵ [%]
51	1	0.03
51	2	0.16
51	3	0.05
51	4	0.12
51	5	0.02
55	1	0.03
55	2	0.16
55	3	0.05
55	4	0.13
55	5	0.02

Table 6.6: Relative error on frequency base between Nastran and WB model - blisc - Tip Free

Even this model appears in accordance to Nastran procedure, meaning that

by running new modal analyses in WB will lead to consistent results.

Downstream the definition of the WB procedure to run modal analysis for LPT blades, the workflow has been refined with several tests in order to individuate the most robust one suitable for the parametric approach. Due to the complexity of the complete rotor stage, the principal effort has been concentrated on the Vane stage; the goal was to define the settings to better generate the mesh in order to work with a not to *heavy* model, but keep robustness of the results.

Chapter 7

The tool *PRIME*

7.1 The parametric templates for Vane model

The most important bottle neck in joining aerodynamic and structural design is the definition of the CAD model. The aerodynamic analyses are based on Computational Fluid Dynamics, so for their purposes the blade profile that matters is the one that interacts with the airflow. For structural analyses, it is required to complete the profile with boundaries, in order to simulate the contact models. This point needs a dedicated designer that can draw and fix IB and OB.

This is a very time consuming operation and does not allow the automation of the process.

To solve the problem, a parametric approach for boundaries definition might be a suitable path; the models might be generated as function of sets of parameters in order to easily manipulate the global size:

1. The body is defined by means of customizable lengths, thicknesses and angles: by modifying the values, the part assumes different shapes.
2. A scale factor related to the A/F is associated to the body: by choosing a different stage (i.e. blade), the drawing is properly adapted.

The CAD which respond to these characteristics are defined as *templates*.

7.1.1 How to generate a template

For the purpose of this work, the template is meant to be a CAD representing inner and outer band of the vane stage, drawn by means of a parametric criterion. The main concepts behind its generation are:

1. To be representative of the consistent geometry.
2. To employ simple expressions for size definition.
3. To be scaled on a factor related to the A/F.

To answer to point 1, the template is first shaped with reference to a real geometry (i.e. an existing engine): in this case the boundaries of a vane stage.

Due to the geometrical characteristics of the row, the OB and IB can be generated through a standard procedure; these parts might be assumed to be obtained from a basic cross section which is further revolved about the machine axis of rotation by an angle equal to the pitch of the sector. Then, the shape is refined with trimming operations.

Being able to manage this kind of templates, it might be possible to define a loop in order to import the A/F and boundaries geometry in a unique workspace and then opportunely fix them to generate the final CAD for FEM analysis. This idea is strongly consistent since, with the proper settings, it possible to obtain a very realistic geometry and simulate the mechanical behavior with positive output.

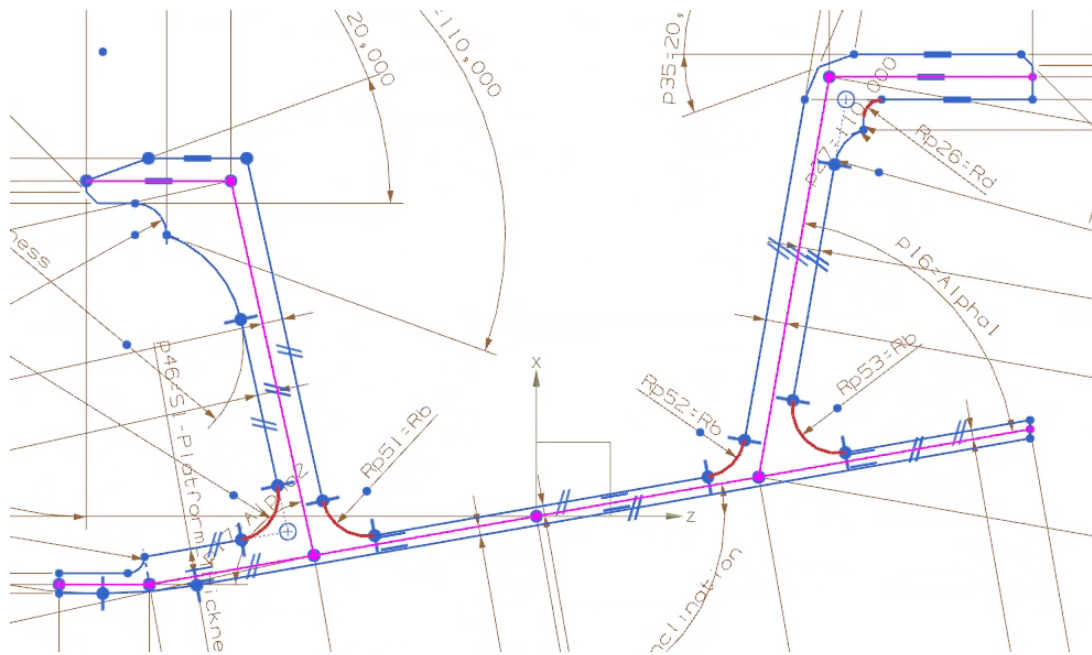


Figure 7.1.1: Example of template

With reference to fig. 7.1.1, the main cross section of the template is split in two parts:

- *skeleton*, the fuchsia part, is a rough representation, but complete, of the cross section in order to enlighten heights, lengths and angles; it is used to manage the gross size of the template through sets of parameters.
- *scaffold*, the blue part, gives consistency to the cross section with all the proper details; it is constrained to the skeleton in order to be adaptable.

The 2D sketch is, thus, revolved in order to get a 3D object and then trimmed according to the pitch extension.

7.1.2 The tool *DynBooster*

In the Avio Aero library instruments for LPT preliminary design there is a tool developed in the past for the handling of turbine profiles through a parametric

approach.

DynBooster is a GUI based on C++ language able to manage the CAD generation in an automatic way by means the setup of a number of parameters. The tool recalls, basically, suitable functions of the platform *Unigraphics NX* to manipulate the A/F and the templates.

At the end of the *Aero* design, the outcome is the shape of the airfoil in form of a set of 2D cross sections and swirling trend of the profile. The tool can read this information and generate in NX workspace the 3D body of the blade.



Figure 7.1.2: Airfoil generated through a set of 2D cross sections

Beside, many other parameters are read from the input file which are required for the correct manipulation of the templates, as:

- Radial distance from the machine axis of rotation of tip and hub;
- The chordal lengths;
- The leading and the trailing angles.
- The inclination of the A/F section at the boundaries.

Defined the template and the stage under investigation, the CAD is scaled with respect to the proper blade. Then, the user is able to manipulate the detailed geometry through a set of parameters such as the ones displayed in fig. 7.1.1.

Once the OB and IB are customized, they have to be properly fixed to the A/F and successively blended; this operation is not straightforward since a wrong positioning might lead to an incorrect dynamic behavior of the structure. Moreover, the crucial point is to find a way to automatically iterate this procedure.

The solution is anyhow very intuitive; from one side, the template is provided of a *gross point* which acts as a reference where its frame is based. On the other end, DynBooster *generates* a rough 2D cross section of the tip (equivalently for the hub) starting from relevant points of the blade profile: *leading edge, high curvature, maximum thickness, mid-chord* and *trailing edge*.

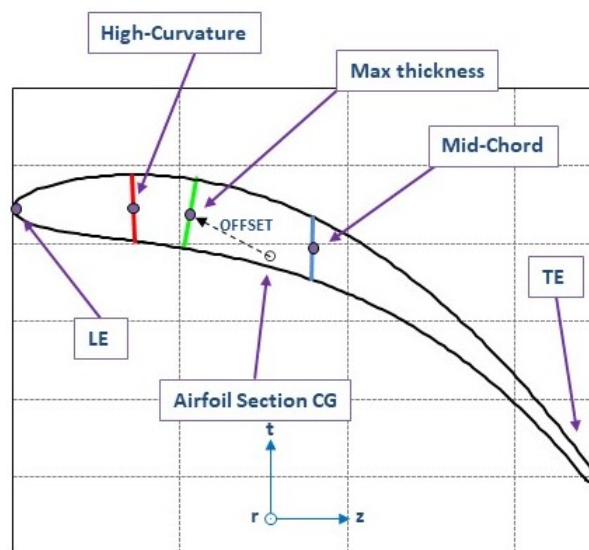


Figure 7.1.3: Template centering

The template is first properly inclined and then fixed in the *center of gravity* of the airfoil section; this position is not the correct one and various tests showed the best results by setting the part in the point of maximum thickness of the blade: the tool computes, thus, the axial and tangential offset between the two points, then moves the template through the basepoint (see fig. 7.1.3).

Finally, the part and the airfoil are blended. It is important to stress that the latter operations are not executed by the user, but are managed by the tool itself.

The parameters that manipulate the template are subdivided into two groups:

1. *System Parameters*, are transparent to the user and are set by the tool in order to properly scale and move the template.
2. *Custom Parameters*, regard the variables that allow to modify the shape in terms of height, inclinations of hooks, thicknesses, etc.

Any choice can be, in first approximation, totally arbitrary; moreover, since PRIME is thought to be a multidisciplinary tool the user might not be fully confident on the manipulation of the template and get inconsistent results. To avoid this, DB has been updated with a very simple but efficient control loop based on the bisection rule.

The template is first scaled with reference to the chordal length: if the user does not customize the setting, the result is a consistent geometry for OB and IB. On the other end, the variables of the CAD might modified by means of a GUI in a very intuitive way; in this case, the tool evaluates the parameter variation and selects the correct way to update the geometry. The control loop compares the *default* value and the entered one and computes the absolute variation: if the parameter is less than doubled, the CAD is updated with the new dimension; otherwise, it is defined a number of steps n and the geometry is iteratively updated. At any check, the part is modified and if no warnings are returned the variable is frozen with the closest value to the set one. The workflow followed by the loop is , thus, shown:

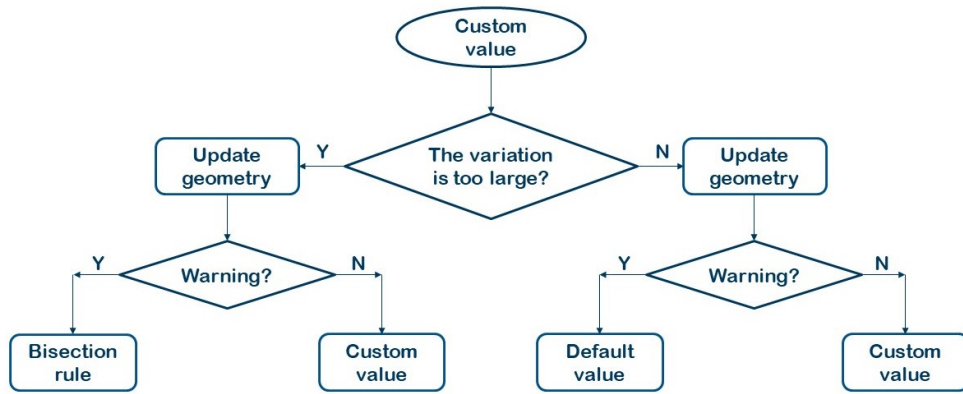


Figure 7.1.4: Template updating workflow

The shape for OBV and IBV are shown as follows:



Figure 7.1.5: Parametric template for OBV

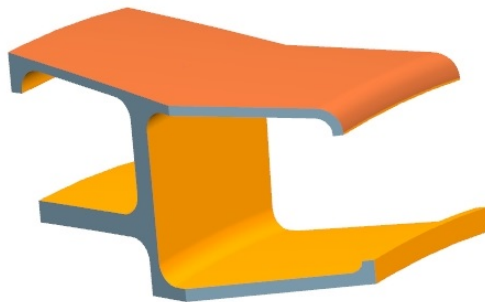


Figure 7.1.6: Parametric template for IBV

The final step is the definition of proper *Named Selection* in the template; they represent tags for specific surfaces that might be read by WB in order to

handle and model the geometry.

7.2 The WB wizard for *FEM*

The modeling of a vane sector is a quite simple process since there are not particular requirements in terms of grid size - no cyclic symmetry - and BCs - no centrifugal stress. Strictly speaking, three are the main steps to follow:

1. Grid generation: with no cyclic symmetry requirements.
2. Application of the thermal load.
3. Setting of BCs at the IB and OB: grounded contact surfaces.

These actions might be automated since the procedure is standard, especially for the preliminary design; in addition, WB allows to program a *wizard*, a GUI, to iteratively run determinate sequences. Then, it is possible to make use of Named Selection opportunely set in NX to enlighten relevant geometric features to automatically manage the model in terms of constraints and solution postprocessing. The features configured in NX and used in WB are, thus, shown below:

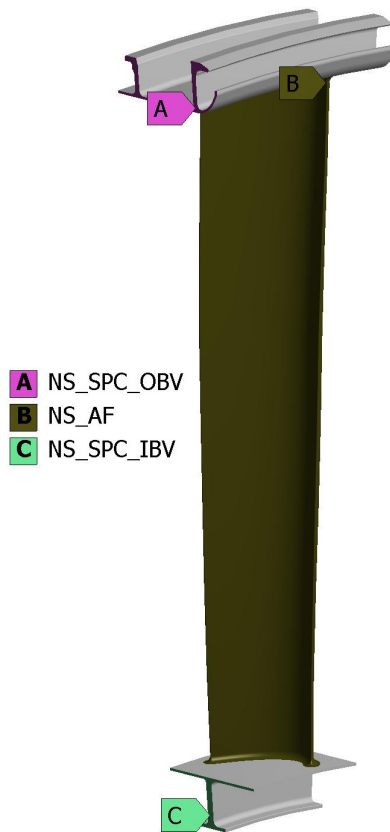


Figure 7.2.1: Model in WB through the Named Selection created in NX

The grid is automatically generated and elements sized for a dynamic analysis.

The boundaries contact faces are grounded through the feature *Nodal Displacement*. The thermal load is imported in form of a 1D radial temperature map.

In fig. 7.2.1 is shown, beside the Named Selection for OB and IB, a selection for the airfoil; this surface is used during the postprocess: in fact, for flutter check it is required to enlighten the modal displacements of the nodes which interacts with the fluid. This way, once the modal analysis is done, it is straightforward to extract the information through this feature and generate the input files for flutter tool.

The solution is then calculated with the possibility to run several operating points: this way, *COLD*, *CRUISE* and *TAKEOFF* configuration might be simu-

lated by uploading three different thermal loads. Downstream, the responses are classified on frequency basis to generate the Campbell diagram.

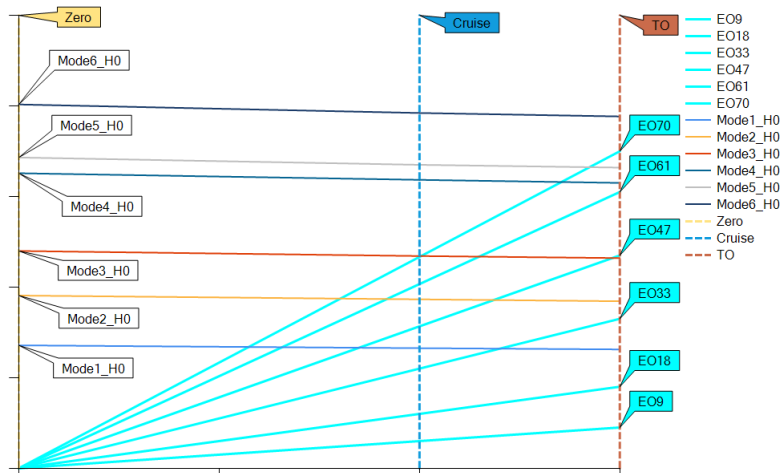


Figure 7.2.2: Campbell diagram generated downstream the PRIME procedure

Beside the fig. 7.2.2, the tool prints a text file reporting the crossings of the diagram.

Another possible output of the tool is the input file for flutter analysis; starting from the Named Selection of the airfoil, it is possible to extract the modal displacements of the associated grid nodes in order to run, downstream, the flutter check. This possibility has been implemented in order to connect, in the future, the flutter tool to PRIME.

To summarize, the Workbench *wizard* which is in fact the core of the tool PRIME, performs the below listed actions:

1. Generation of the geometry of the vane with proper features by recalling the tool *DynBooster*.
2. Selection of the material from a database.
3. Choose of the desired outputs, Campbell diagram and/or input for flutter analysis.
4. Setting of the *rpm* for Cold, Cruise and Takeoff and the associated temperature maps.

At the end, the wizard returns a WB model with the three prestressed modal analyses: if needed, further investigations can be operated from these starting points by launching *ANSYS Mechanical*; beside, in the working folder, all results are properly summarized and modeshapes screenshots available for consulting. If requested, the Campbell diagram and flutter inputs are saved too.

On the other end, if the CAD model for vane is already available it might be directly processed in PRIME without recalling DynBooster; it is required, in this case, to work with a NX file where the geometrical features (i.e. tags for faces) are manually set. Then, by launching PRIME the tool will be directly fed by the geometry: the downstream procedure keeps unchanged.

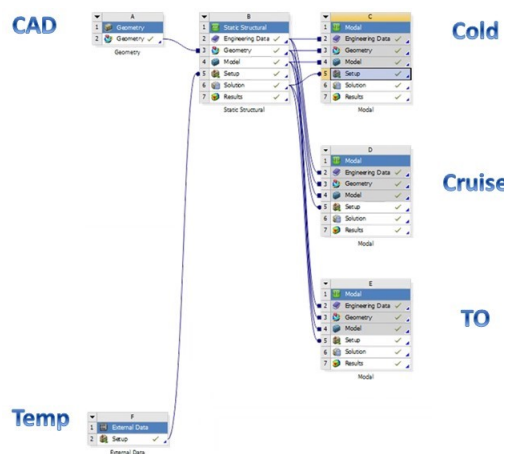


Figure 7.2.3: WB project automatically generated through the tool PRIME

The estimated advantages with the proposed process are very impressive, since it is expected a computational time reduction higher than the 90%; the entire procedure might be run by one user from the CAD generation to the modal analysis, so it is possible to maintain the global overview of the workflow. In case of not positive results from structural point of view, it is only requested to modify the aerodynamic profile and launch the tool: in the time window of 20' it is possible to obtain a feedback and appreciate the goodness of the proposed modification. This way, by integrating PRIME in the *Aero* design loop, aerodynamics and structural mechanics merge: an *Aero-Mech* optimization loop is, thus, available; the result would lead, at the end, to the definition of an aerodynamic profile which responds

both from performance and structural point of view already at preliminary design phase. Strictly speaking, an optimized profile means a lighter engine, so a greater *pay load*.

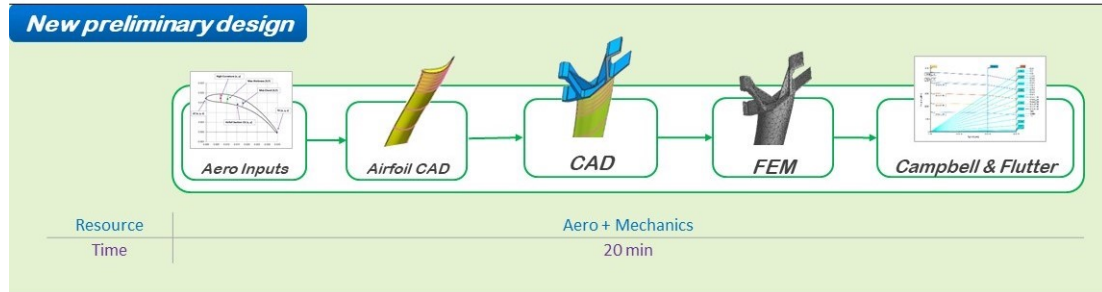


Figure 7.2.4: PRIME workflow

7.3 Vane in *PRIME*

As far as concerned the vane model, the workflow followed in PRIME is the same investigated in paragraph 6.1; by the way, the tool performs the entire procedure in automatic way, so any refinement is not allowed, especially regarding the mesh generation. For validation, the modal analysis results have been compared with the manual approach.

Since the process might include the automatic CAD generation by means of the templates, the geometry shown in fig 6.1.1 has been replaced with a new one managed inside DynBooster. From this input, the FEA has been run in Nastran first, then the bdf imported in WB for the first check; finally, the same geometry has been processed in PRIME through the automatic approach.

It is important to stress that the *automatic* grid is the 60% coarser than the one generated by hand. The result, based on the first six modeshapes, are computed through the eq. 6.1 and shown in tables 7.1 and 7.2.

<i>Mode</i>	ϵ [%]
1	0.01
2	0.05
3	0.06
4	0.09
5	0.15
6	0.20

Table 7.1: Relative error on frequency base between Nastran and WB model - vane, manual grid

The two solutions are almost coincident, since the relative error is deeply lower than 1%, showing, again, the goodness of the WB procedure. The MAC analysis shows the full modal correlation too.

The same geometry is, then, processed through the tool PRIME; the error is computed with reference to Nastran results.

<i>Mode</i>	ϵ [%]
1	1.64
2	1.52
3	1.00
4	0.59
5	0.40
6	0.74

Table 7.2: Relative error on frequency base between Nastran and PRIME model - vane, manual grid

For this comparing, the errors are not as low as the ones shown in table 7.1, by the way, they are consistent for mainly two aspects:

- The meshes are consistently different, so it is expected a frequency variation

of few Hz .

- The absolute variation, by employing the eq. 6.1, is more incident for lower frequencies (i.e. first modes), as the trend shows.

In conclusion, the process is validated even if it might be refined in many aspects, starting from the grid generation: for example, by means of a detailed setting of the Aggressive Mechanical meshing function.

7.4 Blade Only in *PRIME*

More than once it has been stressed that vane and simplified blade are modeled in a similar way. For this, it is mainly straightforward to update the *WB wizard* to run the modal analysis for the blade; for brevity, only the tight contact model has been defined, even if it is possible to implement all the other configurations. Two modifications are required:

- Cyclic symmetric grid at interlocking interfaces, even if no cyclic symmetry is involved.
- The *rpm* set for Cold, Cruise and Takeoff represents a centrifugal load for the prestressed modal analysis.

On the other end, the geometry of the blade is more complex and the definition of the parametric templates is not straightforward; moreover, they may be considered three parts, since the Inner Band is split into dovetail and shank.

For that reason, the process has been investigated with a *real* geometry manually set with the proper NS discussed for the vane model.



Figure 7.4.1: Blade manually set with proper Named Selections

With reference to fig. 7.4.1, the red region is the interlocking interface where, through the feature *Face Meshing*, it is possible to force the correspondent 2D grids to be symmetrical; here the faces are grounded. The green region, instead, is the contact interface with the disc where no relative motion is allowed.

The downstream procedure, then, is identical to the one for the vane with the only exception of the centrifugal load to be taken into account.

The comparing Nastran-WB-PRIME process has been the same shown for the vane sector.

<i>Mode</i>	ϵ [%]
1	0.15
2	0.12
3	0.05
4	0.00
5	0.16
6	0.03

Table 7.3: Relative error on frequency base between Nastran and WB model - blade only, manual grid

The table 7.3 shows the relative error between the Nastran and WB model

on the same mesh for the blade only model: the values are significantly lower than the 1% so the match is verified; in addition, also the MAC analysis shows positive results.

<i>Mode</i>	ϵ [%]
1	0.73
2	0.74
3	0.54
4	0.94
5	0.65
6	0.59

Table 7.4: Relative error on frequency base between Nastran and PRIME model - blade only, manual grid

The automatic grid generated in PRIME is 75% coarser than the manual one, so it is expected not to see coincident results; anyhow, the relative error is lower than the 1% for all the modes taken under investigation, showing the goodness of the tool resolution even for the blade only model.

Since the blade only model showed the same potential as the vane, it has been started a study to generate parametric templates for the blade representing shroud, shank and dovetail. Beyond the necessity to work with consistent shapes, the crucial point is the update of DynBooster in order to be able to manage three different templates: for vane, only OB and IB. The step is not straightforward, but pave for a good result has been traced.

Conclusions

This thesis was meant to propose a new simulation method for preliminary design of LPT rows, aiming to define a procedure in order to perform in parallel the aerodynamic and structural mechanic design. The final goal is to give fast mechanical feedback inside the blade profile optimization loop in order to design the airfoil also looking to structural thresholds.

To this purpose, the preliminary analyses concerning the free response of the system have been performed in Ansys Workbench; in this workspace, a *wizard* has been programmed to iteratively run the sequences to set the FEM model and automatically post process the solution. The geometry has been managed with a tool of Avio Aero, DynBooster, able to generate the CAD through a parametric approach.

At the end, the processing time for preliminary structural mechanics is consistently reduced, about 90%, allowing to perform in advance more detailed analyses such as the Campbell diagram generation. By integrating this tool, *PRIME*, downstream the airfoil optimization loop, it is possible to iterate the first *Aero-Mech* preliminary design, where the profile is not only investigated regarding the performance, but also the mechanical response.

This way, the design process might be controlled from an unique point of view, allowing the reduction of errors and misunderstandings. The final frozen geometry for manufacturing would be, thus, the *optimus* between the aerodynamic and structural preliminary assessments, leading to the reduction of fixings in the detailed design phase.

For the complexity of the system, the method has been refined first for vane model; anyhow, aiming to implement the real blade geometry, an introductive study for

the rotor stage has been proposed, showing interesting results in line with the ones of the nozzle model.

References

Books and Papers

- **J. D. Mattingly, W. H. Helsner, D. T. Pratt:** *Aircraft Engine Design*, second edition, Reston, VA 20191: AIAA Education Series, 2002.
- **P. G. Hill, C. R. Peterson:** *Mechanics and Thermodynamics of Propulsion*, second edition, Addison-Wesley Publishing Company Inc., 1992.
- **P. Mc Comb:** *Dynamics of a Simple Rotor System*, SRDD, 2013.
- **R. L. Bisplinghoff, H. Ashley, R. L. Halfman:** *Aeroelasticity*, Dover Books on Aeronautical Engineering, Dover Publications, 1996.
- **A. V. Srinivasan:** *Journal of Engineering for Gas Turbines and Power: Flutter and Resonant Vibration Characteristics of Engine Blades*, Worcester Polytechnic Institute, Presented at the International Gas Turbine & Aero-engine Congress & Exhibition, Orlando, Florida, 1997.
- **P. Polach:** *Calculation of Natural Vibration of a Steam Turbine Bladed Disk Using Rotational Periodicity*, SKODA VYZKUM, 2008.
- **P. Polach:** *Dynamics of Machines: Evaluation of the Suitability of the Bladed Disk Design Regarding the Danger of the Resonant Vibration Excitation*, Section of Materials and Mechanical Engineering Research, Prague, 2011.
- **D. H. Hodges, G. A. Pierce:** *Introduction to Structural Dynamics and Aeroelasticity*, second edition, Cambridge Aerospace Series, Cambridge University Press, 2014.

- **D. Vogt, T. Fransson** *Aeroelasticity of Turbomachines*, Toulouse, France, 2013.
- **G. Genta**: *Vibration Dynamics and Control*, Springer, New York, 2009.
- **G. Genta**: *Dynamics of rotating Systems*, Springer, New York, 2005.
- **A. Fasana, S. Marchesiello**: *Meccanica delle Vibrazioni*, CLUT, Torino, 2006.
- **L. Casalino, D. Pastrone**: *Fondamenti di Macchine*. Academic notes, Politecnico di Torino, A.Y. 2013-2014.
- **L. Casalino, D. Pastrone**: *Motori per Aeromobili*. Academic notes, Politecnico di Torino, A.Y. 2014-2015.
- **C. M. Firrone**: *Dynamic behavior of cyclically symmetric solids for aeronautical applications*. Industrial Academy Program on Manufacturing and Technologies, Politecnico di Torino.
- **M. Furfaro**: *Stabilizzazione di Rotori in presenza di Fenomeni Aeroelastici Critici per mezzo del Mistuning Intenzionale*. Master thesis, Aerospace Engineering, Politecnico di Torino, 2015.
- **F. Musso**: *Validazione di un nuovo modello di contatto all'interlocking per stadi di turbine di bassa pressione*. Master thesis, Aerospace Engineering, Politecnico di Torino, 2016.
- **A. Ramieri**: *Analisi e comparazione di diversi modelli di contatto all'interlocking per rotori di turbine di bassa pressione*. Master thesis, Aerospace Engineering, Politecnico di Torino, 2017.

Utilities and Websites

- **Ansys Workbench User's guide**.
- **Siemens NX 10 documentation**.